



Experimental and numerical studies on film cooling with reverse/backward coolant injection



Kuldeep Singh, B. Premachandran*, M.R. Ravi

Department of Mechanical Engineering, Indian Institute of Technology Delhi, Hauz Khas, New Delhi, 110016, India

ARTICLE INFO

Article history:

Received 3 February 2016

Received in revised form

21 September 2016

Accepted 22 September 2016

Keywords:

Film cooling

Forward hole

Reverse hole

Injection angle

Discharge coefficient

ABSTRACT

The conventional forward injection for film cooling with cylindrical holes, where the axial component of the coolant velocity is aligned with mainstream flow direction creates kidney vortices. This results in quick mixing of the coolant with the mainstream. The conventional anti-kidney vortices cooling holes require shaping or branching which adds to the cost and complexity of the system. In this paper, reverse/backward injection is proposed to improve film cooling. In the case of reverse/backward injection the secondary air is injected such that its axial velocity component is in the reverse direction to that of the mainstream. Film cooling is studied experimentally and numerically on a flat plate with forward and reverse injection. The injection angle of the cooling hole is varied from 30° to 60° in both forward and reverse directions at five blowing ratios ranging from 0.25 to 3.0 at a fixed density ratio of 0.91. The length to diameter ratio of the cooling hole is kept at 5 and the mainstream Reynolds number is maintained at 3.75×10^5 . Film cooling effectiveness obtained with the reverse holes is found to be much higher than that of the forward holes. Improvement in the area weighted average values of film cooling effectiveness for blowing ratio, $M = 1$ is 170%, 78% and 186% for injection angles 30°, 45° and 60° respectively. Coefficient of discharge obtained from reverse injection is found to be smaller than that of forward injection. The film cooling effectiveness in the case of reverse injection is found to be less sensitive to the injection angle.

© 2016 Elsevier Masson SAS. All rights reserved.

1. Introduction

Film-cooling is used extensively in gas turbine engines for cooling of components exposed to hot gases. In film-cooling, relatively cold secondary fluid is injected into the hot flow through holes on the surface of the component. The injected cold fluid displaces the hot fluid and forms a layer between the surface to be protected and the hot gases. A coolant layer extends in the downstream direction for a distance determined by the mixing of coolant with the hot gases [1].

In film-cooling, the holes from which the secondary fluid or the coolant is injected are inclined with reference to the surface to be cooled. The flow separates from the wall fluid just downstream of the injection hole and splits into counter rotating vortices, popularly known as kidney vortices [2]. These vortices are influenced by the operating parameters and hole design. Operating parameters such as blowing ratio, density ratio and momentum flux ratio affect

the generation and growth of kidney vortices [3]. Out of the design parameters, the hole inclination, orientation and shape influence the growth of kidney vortices [4]. The presence of kidney vortices increases the mixing of secondary fluid with the hot mainstream. Hence, kidney vortices must be minimized or eliminated to maintain maximum coverage of the surface with coolant film and hence better film cooling. In order to suppress the generation of kidney vortices, to avoid the lift off of secondary fluid jet and the associated undesirable effects, shaped holes are used in the film cooling.

The study of Goldstein et al. [5] is recognized as the first investigation of shaped holes in film cooling studies. The shaped holes have circular cross section which acts as throat or metering section, while the outlet end of the cooling hole is shaped as a diffuser with a divergence angle 10°–15° in the lateral direction as well as in the flow direction [6]. Based on the expansion of the hole, shaped holes are classified as: ‘fan-shaped’, if the expansion is in the lateral direction, ‘laidback’ if the expansion is in the direction of the surface. The purpose of expansion of the hole is to reduce the momentum of the secondary fluid which in turn decreases the penetration and hence mixing of the secondary fluid into

* Corresponding author.

E-mail address: prem@mech.iitd.ac.in (B. Premachandran).

Nomenclature		Greek symbols
C_d	discharge coefficient non-dimensional	α injection angle, in degrees
D	hole diameter, m	η Adiabatic effectiveness, $\frac{T_{ms}-T_w}{T_{ms}-T_{sec}}$
FH	forward hole	ρ density, kg/m ³
m	mass, kg	μ dynamic viscosity, Pa-s
M	Blowing Ratio, $\frac{\rho_{sec}U_{sec}^2}{\rho_{ms}U_{ms}^2}$, non-dimensional	λ characteristic length of test section, m
p	pressure, Pa	
P	hole spacing(pitch) in lateral direction, m	
Re	Reynolds number based on mainstream flow, $\frac{\rho U_{ms}\lambda}{\mu}$	
RH	reverse hole	
T	absolute temperature, K	
TR	temperature ratio, $\frac{T_{sec}}{T_{ms}}$, non-dimensional	
U	mainstream velocity, m/s	
V	coolant hole velocity magnitude, m/s	
X	streamwise coordinate, m	
Z	spanwise coordinate, m	

mainstream fluid.

Haven and Korosaka [4] investigated film cooling over a flat plate with cylindrical and shaped holes. They showed that kidney vortices are formed when the secondary fluid is injected through cylindrical holes which diminish film cooling performance. This study also revealed that the effect of kidney vortex can be decreased by using shaped holes. In shaped holes anti-kidney vortices were formed which suppress the jet lift-off [4].

The study of Gritsch et al. [7] provided a comparative analysis of cylindrical holes, fan-shaped holes and laidback fan-shaped holes. The laidback fan-shaped holes are the combination of both fan-shaped and laidback holes. This study highlighted that the film-cooling performance of fan-shaped holes is better than cylindrical holes and the performance of laidback fan-shaped holes is the best among all investigated hole shapes. Bell et al. [8] investigated shaped holes in combination with compound angle holes. Five hole configuration viz. (i) cylindrical round simple angle holes, (ii) laterally diffused simple angle holes (iii) laterally diffused compound angle holes, (iv) forward diffused simple angle holes, and (v) forward diffused compound angle holes were investigated. The simple cooling holes were inclined at an angle with the flow direction. In case of compound angle holes, the cooling holes were given some inclination in lateral direction as well. All the shaped holes were found to be better in terms of spread of the cooling film over the surface to be cooled, as compared to cylindrical holes. The best film cooling performance was found for the case of laterally diffused compound angle holes followed by forward diffused compound angle holes. They claimed that the improvement in film cooling effectiveness is partly due to film diffusion from expanded hole shapes and partially due to increased lateral spreading of injectant from compound angles.

Saumweber et al. [9] studied the effects of free-stream turbulence on film cooling with shaped holes over a flat plate at a fixed density ratio of 1.7. They concluded that at low turbulence levels, the shaped holes do not show any detachment from the surface even at the highest investigated blowing ratio i.e. M = 2.5. The momentum of the coolant decreases because of the expanded exit and hence the penetration of secondary fluid into the mainstream decreases. Silietti et al. [10] studied numerically film cooling over 3D gas turbine endwall with one fan-shaped cooling hole. A comparison of film cooling effectiveness in adiabatic and conjugate heat transfer mode was done for blowing ratio, M = 1 and coolant to mainstream temperature ratio of 0.54. The studies of Cho and Rhee

[11], Yu et al. [12], Taslim and Khanicheh [13], Colban et al. [14], Lee and Kim [15], Wright et al. [16] on shaped hole re-iterate that the hole shaping improves the film cooling performance.

Shaped holes increase the complexity and cost of the system. In order to simplify the design of cooling holes, Dhungel et al. [17] proposed branched cooling holes. These holes are cylindrical in shape and after a certain distance from the inlet side, two symmetrical holes branch out from the main holes. Because of the branching of the holes, the momentum of the coolant decreases at the outlet of cooling holes. They claimed that the branched holes act as anti-vortex holes and reduce the effect of kidney pair vortices, which leads to better film coverage in both downstream and lateral directions compared to conventional cylindrical holes. A recent numerical study by Khajehhasani and Jubran [18] on branched holes also showed a significant reduction in the jet lift-off effect in comparison with the cylindrical and forward-diffused shaped holes.

In the quest of reducing the jet lift off and kidney vortices Lu et al. [19] investigated cylindrical holes with trenches. They studied the effect of the trench width and depth on film cooling from cylindrical holes embedded in trenches using a transient IR thermography technique to measure the heat transfer coefficient and the film effectiveness. They concluded that trenching the holes in a slot reduces the jet momentum at the exit, spreads the jet and provides 2D jet coverage compared to 3D nature of individual jets, providing better overall film cooling effectiveness.

The walls of gas turbine blades are usually thick and it is feasible to make shaped holes in the geometry of this kind. However, the combustion chamber liner and the wall of afterburner section of fighter planes, which also make use of film cooling, are very thin. Hence, it is not feasible to make shaped holes in these geometries. The shaped holes also add to the cost and complexity of manufacturing. Yang and Zhang [20] investigated a row of holes with ridge-shaped tabs. They found that the presence of the ridge-shaped tabs in the nearby region of the primary film cooling holes mitigates the primary vortices. The ridge-shaped tabs provide enhancement in cooling effectiveness but at the expense of larger pressure drop. They admitted that such holes are difficult to manufacture not practical for use in practical applications.

Cooling of combustion chamber and the afterburner section of a gas turbine engines is still a challenge because of their thin cross section. The operating blowing ratio and density ratio is also high for these components compared to that for turbine blade cooling.

High blowing ratio increases the jet lift-off of secondary fluid which further adds to the complexity of the cooling system.

The present work aims at designing coolant injection holes in such a way that the problem of generation of kidney vortex structure and the design difficulties are resolved while using simple holes. The cooling hole used in the present work is designed in such a way that it ejects coolant in upstream direction making an acute angle with the wall, referred to as reverse holes/backward holes hereafter in this paper.

Li et al. [21] carried out numerical and experimental studies on cooling holes inclined at an angle 30° in the backward direction and compared the results with a cooling hole inclined at an angle 30° in the forward direction. The numerical studies were carried out on a flat plate as well as on an airfoil while the experimental study was conducted on a flat plate to validate the numerical models. In the numerical studies, the $k-\epsilon$ turbulence model with enhanced wall functions was used. The numerical study on flat plate was carried out for a blowing ratio (M) of 2 and density ratio (DR) of 2.43. The numerical study on airfoil was carried out for a blowing ratio of 1 and a density ratio of 2.43. The blowing ratio, $M = 1.33$ was used in the experimental study. They reported the spanwise distribution of film cooling at various downstream distances and hole length to diameter ratios. They found that the cooling holes with the backward injection give higher film cooling effectiveness in the spanwise direction. Li et al. [22] also carried out numerical and experimental studies on cooling holes inclined at an angle 30° in the backward direction and compared the results with cooling hole inclined at an angle 30° in the forward direction. In their study, the blowing ratio was varied from 0.3 to 2.0 and the density ratio was varied from 1 to 2. Simple cylindrical holes, compound cylindrical holes, simple fan-shaped holes and compound fan-shaped holes were investigated. They claimed that the backward injection of secondary fluid is not as sensitive to variations of blowing ratios and density ratios when compared to the forward injection. They also showed that the film cooling of both simple and compound angled cylindrical holes is better than that of shaped holes by backward injection. Pressure required in the case of backward injection was found to be more as compared to that for forward injection holes.

Shetty et al. [23] carried out numerical study on film cooling of a curved surface with backward injection. Numerical studies were carried out on a simplified gas turbine blade for a blowing ratio, $M = 1$, density ratio, $DR = 2.42$ and injection angle of 35° . It was reported that the film cooling effectiveness obtained from backward injection decreases with increase in blowing ratio for pressure side and increases for suction side of the turbine blade. Lateral film cooling effectiveness obtained from backward injection was found to be better than that of forward injection but centerline film cooling effectiveness decrease because of backward injection for both convex and concave surfaces.

Park et al. [24] carried out an experimental study on film cooling of a flat surface with forward and backward injection. Two rows of cooling holes were made with pitch 6 d, and row spacing 3 d. Cooling holes were inclined at an angle 35° in both forward and backward direction. The blowing ratio was varied from 0.5 to 2.0 at a fixed density ratio of 1. They found that at higher blowing ratios, film cooling effectiveness obtained from backward injection was much better than that of forward holes. Lateral coverage of backward holes was also better.

Chen [25] experimentally investigated film cooling of a flat surface using simple cylindrical holes, fan-shaped holes with and without compound angle for both forward and backward injection. Effect of blowing ratio and density ratio was investigated for these geometries. The blowing ratio was varied in the range of $M = 0.3$ to $M = 2.0$ and coolant to main stream density ratio was varied from 1

to 2 by varying foreign gas. The free stream turbulence intensity effects were also investigated by varying it from 0.5% to 6%. The results showed that the film cooling effectiveness with backward injection was greatly reduced for shaped holes as compared with the forward injection. However, significant improvements were observed for the case of simple angled cylindrical hole at higher blowing ratios. Backward injection also showed improvements in film cooling effectiveness for compound angled cylindrical holes at the near film-hole regions for higher blowing ratios.

The improvement by the backward injection of the coolant is quite promising. Further investigation is required to understand and to minimize the aerodynamic losses in the film cooling with the backward injection holes. It is evident that the film cooling performance of normal injection angle is poor because of jet lift-off. In both of the above studies [21]–[22], backward 30° injection angle proves better than forward 30° injection angle. It will be very useful to know that which inclination angle in backward direction suppress jet lift-off with lowest pressure drop.

In the present work, film cooling is studied experimentally on a flat plate with forward and reverse injection. The cooling hole injection angle has been varied from 30° to 60° with respect to the flat surface in both forward and backward direction for five blowing ratios (M) ranging from 0.25 to 3.0 at a fixed density ratio (DR) of 0.91. The cooling hole length-to-diameter ratio, L/D is kept at 5 and the mainstream Reynolds number defined based on the mainstream conditions and characteristics length of test section is maintained at 3.75×10^5 . The Reynolds number (Re_d), defined based on hole diameter and mainstream flow conditions is maintained 11250. Numerical study was carried out for the range of parameters for which experimental study was conducted. The flow visualization and pressure drop calculations have been carried out with the help of numerical analysis.

2. Experimental set-up

2.1. Description and calibration of instruments

A schematic diagram of the experimental set-up used in the present study is shown in Fig. 1. In the experiments, it should be noted that film heating is used to simulate film cooling i.e. the secondary air is at a higher temperature than the mainstream. The experimental set up consists of a subsonic open-circuit wind tunnel. In the wind tunnel the ambient air is supplied from a centrifugal blower of 2000 lps capacity which is driven by a 25 hp AC motor. The secondary air is drawn from a tank which is connected to a reciprocating compressor. Before storing the compressed air in the tank, the air is filtered and dehumidified. This compressed air is then supplied to a heater. An air filter and a pressure regulator are mounted upstream of the heater. Using a pressure regulator, the secondary air pressure could be set up to 10 bar. The mass flow rate of the secondary air is controlled by Alicat mass flow controller, MCR-2000SLPM-D-PAR. The metered air from the mass flow controller enters the electrical heater. The heated secondary air is then supplied to the test section through a settling chamber and a plenum. The detailed description of experimental setup, instruments, calibration procedure of the instruments can be found in Singh et al. [26]. Here, test section is explained in detail. The test section is a square duct made up of plexiglass with a cross section of $200 \times 200 \text{ mm}^2$ and the length is 1470 mm. Fig. 2 shows the top view of the test plate, which is placed on the floor of the test section. Test plates are made of Polytetrafluoroethylene (PTFE). The length of test plate is 45D and width inside the test section was 33D, where D is the diameter of the holes on the test plate. A single row of three cylindrical holes of diameter, $D = 6 \text{ mm}$ are drilled on the test plates. The hole spacing in the lateral direction is 18 mm

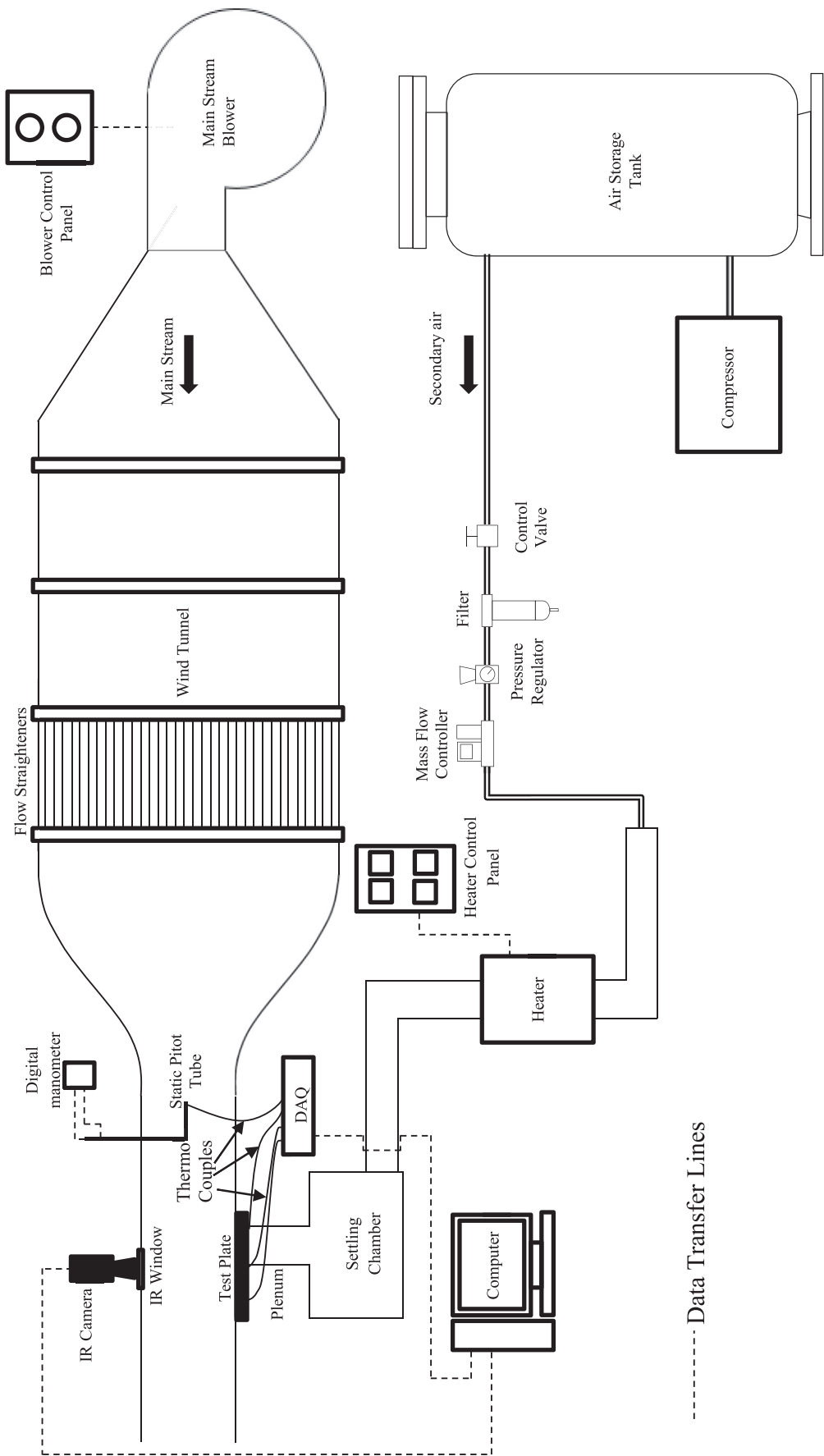


Fig. 1. Schematic diagram for experimental set up.

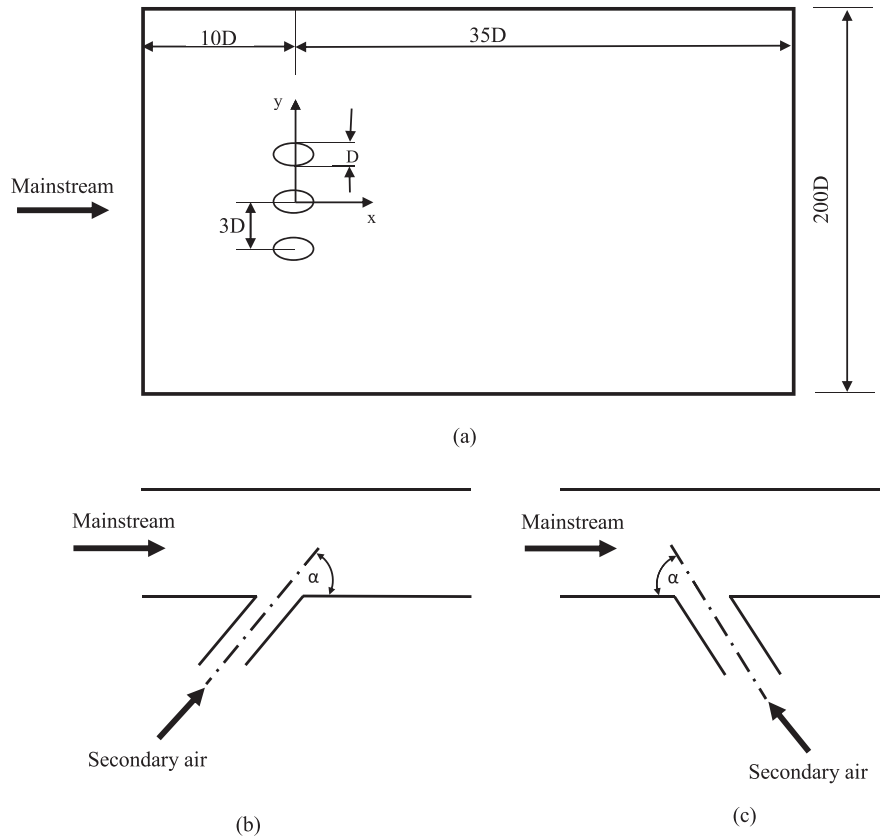


Fig. 2. (a) Dimensions and cooling hole arrangement on test plate (b) forward injection cooling hole (c) reverse injection cooling hole.

and the pitch-to-diameter ratio (P/D) is 3. The angle of the film-cooling holes with the direction of the mainstream flow is varied from 30° to 60° in forward and backward direction for $L/D = 5$, where L is length of each hole. All the experimental studies are carried out at a mainstream Reynolds number (Re_λ) of 3.75×10^5 calculated based on the characteristic dimensions of the test section whereas Reynolds number (Re_d) based on secondary flow and the hole diameter is varied from 2812 to 33750.

2.2. Experimental procedure

The temperature profile of the test plate is measured using an Infrared camera in x-y plane i.e. the plane of test plate. Prior to the data collection, accurately metered secondary air was heated to the desired set temperature and after that the mainstream air was blown in the wind tunnel to a preset velocity. The surface temperature of the test plate was measured using the infrared camera and thermocouples were used for temperature measurement inside the plenum. Mainstream temperature and the surface temperature of test plate at two discrete locations were also monitored using thermocouples in order to verify readings of the infrared measurement. Data acquisition system and Infrared camera were switched on well before data collection to preclude any influence of transient electric heating. Once the bulk temperature of the secondary fluid and surface temperature at the location of thermocouples reached a steady state, data collection was started.

2.3. Data analysis

The flat plate used in the test section is made of a Polytetrafluoroethylene (PTFE) sheet. PTFE sheets have a low thermal

conductivity and hence can be treated as adiabatic wall. The effectiveness of film cooling (heating) of the surface is calculated from the temperature measurement using Eq. (1).

$$\eta = \frac{T_s - T_{ms}}{T_{sec} - T_{ms}} \quad (1)$$

Here T_s is the measured surface temperature, T_{ms} is mainstream fluid temperature and T_{sec} is secondary air temperature. T_s is measured using the IR-camera while T_{ms} and T_{sec} are measured by T-type thermocouples.

The uncertainties in the temperature measurement were calculated based on the procedure of Kline and McClintock [31] and results are reported based on a 95% confidence interval. From Eq. (1), the uncertainty of the adiabatic film cooling effectiveness can be calculated as a function of the constituent measurement uncertainties using Eq. (2).

$$\Delta\eta = \sqrt{\left(\frac{\partial\eta}{\partial T_{sec}}\Delta T_{sec}\right)^2 + \left(\frac{\partial\eta}{\partial T_{ms}}\Delta T_{ms}\right)^2 + \left(\frac{\partial\eta}{\partial T_s}\Delta T_s\right)^2} \quad (2)$$

Using this expression, the maximum estimated uncertainty in adiabatic effectiveness along the centerline of the holes on the test plate was 10% based on Kline and McClintock [27].

3. Numerical model

The objective of the present numerical study is to compare the flow field downstream of the injection holes for both forward and reverse holes and to quantify the pressure losses in these holes. In the experimental studies only mainstream velocity in the tunnel

Table 1
Range of parameters used in present study.

Parameters	Present experimental
D (mm)	6
L/D	5
Injection Angle, α	Forward 30°–60°, Reverse 30°–60°
Density Ratio, DR	0.91–2.5
Mainstream Reynolds number, $Re\lambda$	3.75×10^5
Blowing Ratio, M	0.25–3.0

and temperature on the test plate was measured. The ranges of parameters investigated experimentally are given in Table 1. In order to validate the present numerical model, two cases were selected out of the investigated range of parameters. Numerical simulations are carried out at an injection angle 30°, mainstream Reynolds number, $Re = 3.75 \times 10^5$, L/D = 5, M = 1 and DR = 0.91 for both types of film cooling holes.

3.1. Numerical model, mesh and solution procedure

In the present numerical study a three-dimensional geometry has been considered. The computational domain used in the present study is shown in Fig. 3. All the dimensions are taken as per the experimental set up. The film cooling hole diameter (D) considered in this study is 6 mm. The length of the computational domain is 245D, width and height of the domain is 34D. The computational domain consists of a single row of three cooling holes with 3D pitch. The row of film cooling holes is located at 76D in the downstream direction from the mainstream inlet. The central hole is located at the widthwise center of the computational domain. The secondary fluid emerges from a plenum of 25D × 15D × 15D.

The time averaged continuity, momentum and energy equations are solved for statistically steady, incompressible and turbulent flow using ANSYS FLUENT, a commercial CFD solver which uses a finite volume method. The two equation turbulence model, the Realizable $k-\epsilon$ was used with enhanced wall function to achieve closure of Reynolds stress terms. A second-order upwind interpolation scheme is used to discretize all convective terms of the governing equations. The SIMPLE algorithm of Patankar [28] is used for pressure-velocity coupling. The convergence criterion for the residual of energy equation is set to 10^{-8} and that of all the other above mentioned equations is 10^{-5} .

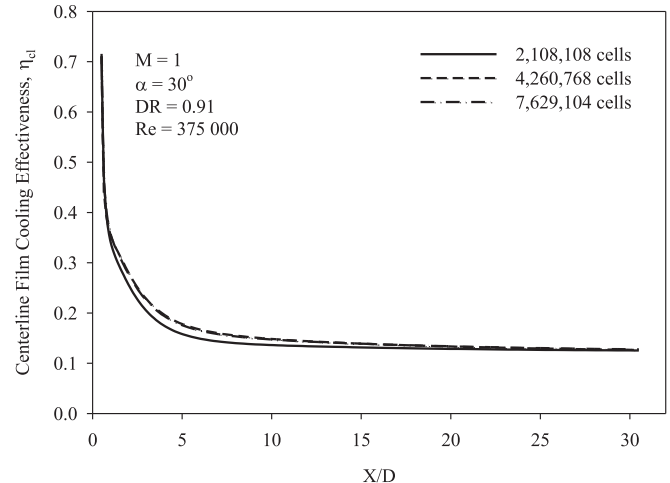


Fig. 4. Grid dependence study using Realizable $k-\epsilon$ turbulence model for Blowing Ratio = 1, $\alpha = 30^\circ$.

3.2. Grid dependence study

Accuracy of the numerical analysis is strongly dependent upon the quality of the grid used. In order to get an optimum grid size, a grid dependence study was carried out. For the present study, non-uniform structured grids were generated using ICEM/CFD. The grids were refined near the walls and the holes to capture the viscous sub-layer. It was ensured that wall y^+ values on all solid walls are less than or close to unity. In order to get grid independent results, three different grids of 2,108,108, 4,260,768 and 7,629,104 elements were compared. The centerline film cooling effectiveness obtained from these three grids is shown in Fig. 4 for blowing ratio of 1, density ratio of 0.91 and mainstream Reynolds number, $Re = 3.75 \times 10^5$.

From Fig. 4, it can be observed that the results obtained with the grid size of 2,108,108 deviates from those using the other two grids, between $X/D = 2$ to $X/D = 20$. The centerline effectiveness curves obtained using the grids with 4,260,768 and 7,629,104 cells overlap with each other at all the downstream distances. Hence, the grid with 4,260,768 cells is selected for further numerical simulations.

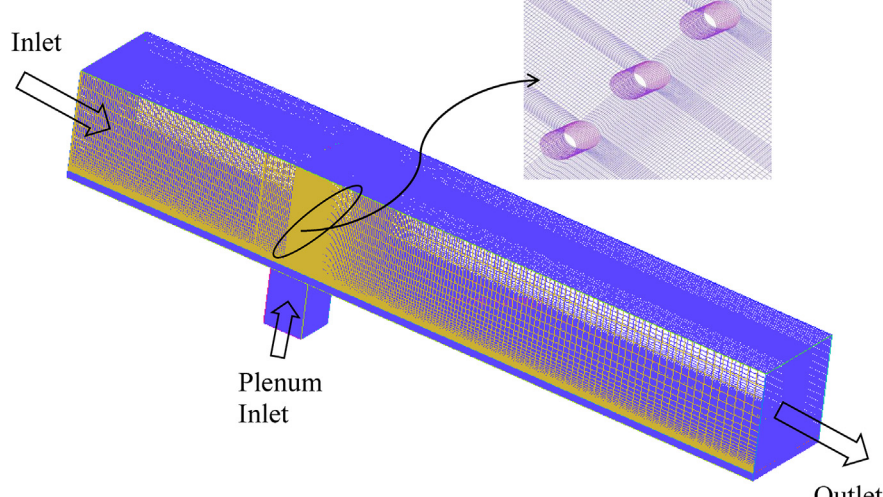


Fig. 3. Typical mesh of computational domain.

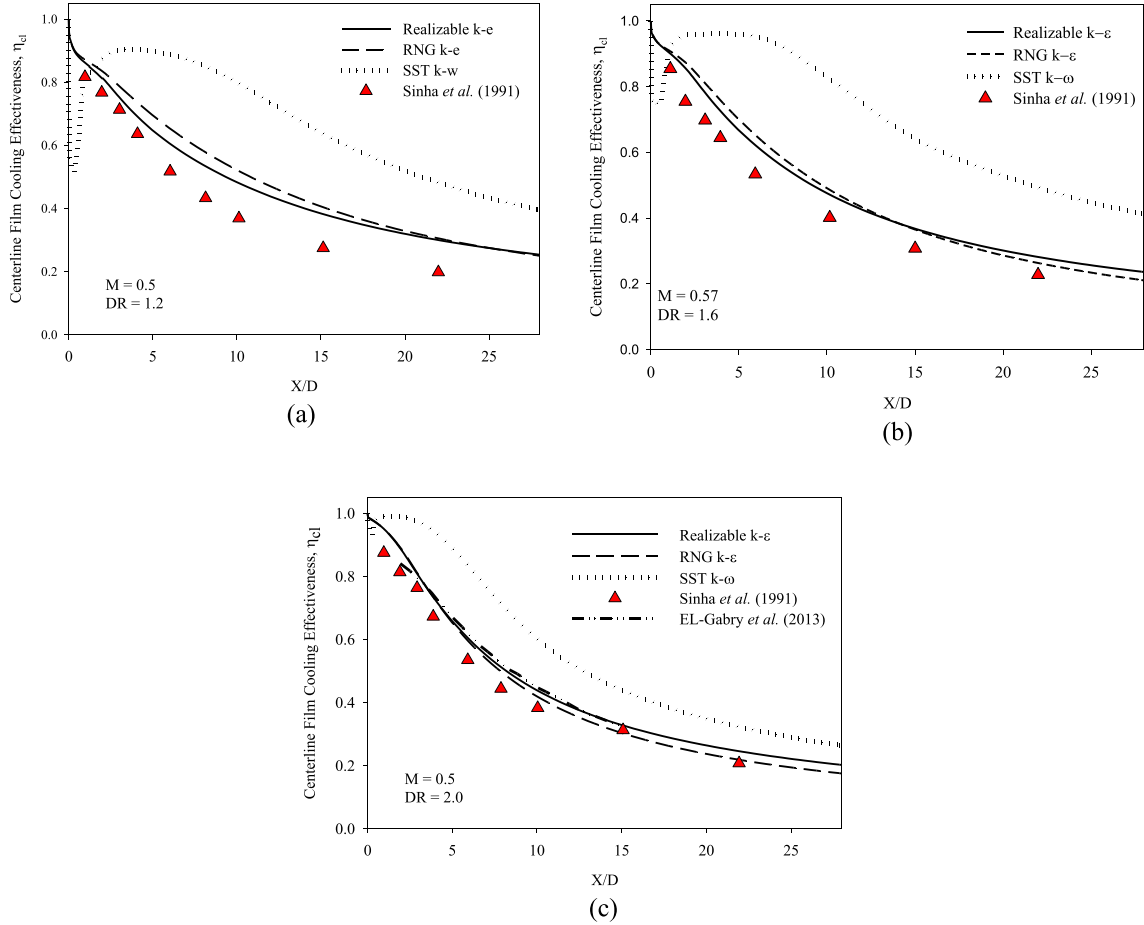


Fig. 5. Comparison of results of present simulation with experimental data of Sinha et al. [1] and numerical simulation of EL-Gabry et al. [5] for (a) $M = 0.5$, $DR = 1.2$, (b) $M = 0.57$, $DR = 1.6$ (c) $M = 0.5$, $DR = 2.0$.

3.3. Validation of numerical model and selection of turbulence model

To validate the present computational model, the results obtained from the present numerical simulations are compared with the experimental results of Sinha et al. [29]. Numerical simulations are carried out for three density ratio, 1.2, 1.6 and 2.0 and corresponding results are shown in Fig. 5. It can be seen from this figure that the results obtained from turbulence models Realizable $k-\epsilon$ and

RNG $k-\epsilon$ are close to the experimental results of Sinha et al. [1]. However, the turbulence model SST $k-\omega$ over-predicts centerline film cooling effectiveness for all the investigated density ratios. In order to cross verify the present computational results, these were also compared with the numerical results of EL-Gabry et al. [30] for $M = 0.5$, $DR = 2.0$. The results for centerline film cooling effectiveness for present and EL-Gabry et al. [30] indicate close agreement. Present numerical results are marginally closer to the experimental results as compare to that of obtained by EL-Gabry

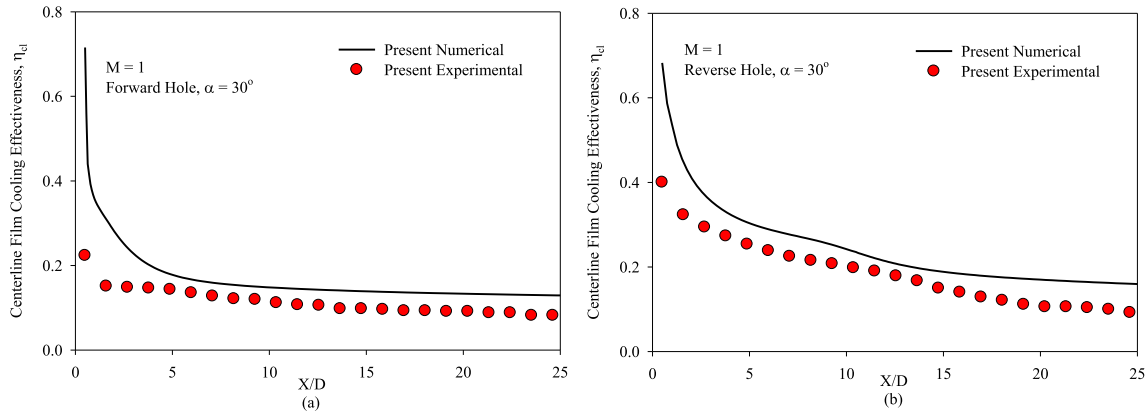


Fig. 6. Comparison of centerline film cooling effectiveness obtained from experimental and numerical studies (a) forward hole, $\alpha = 30^\circ$ (b) reverse hole, $\alpha = 30^\circ$.

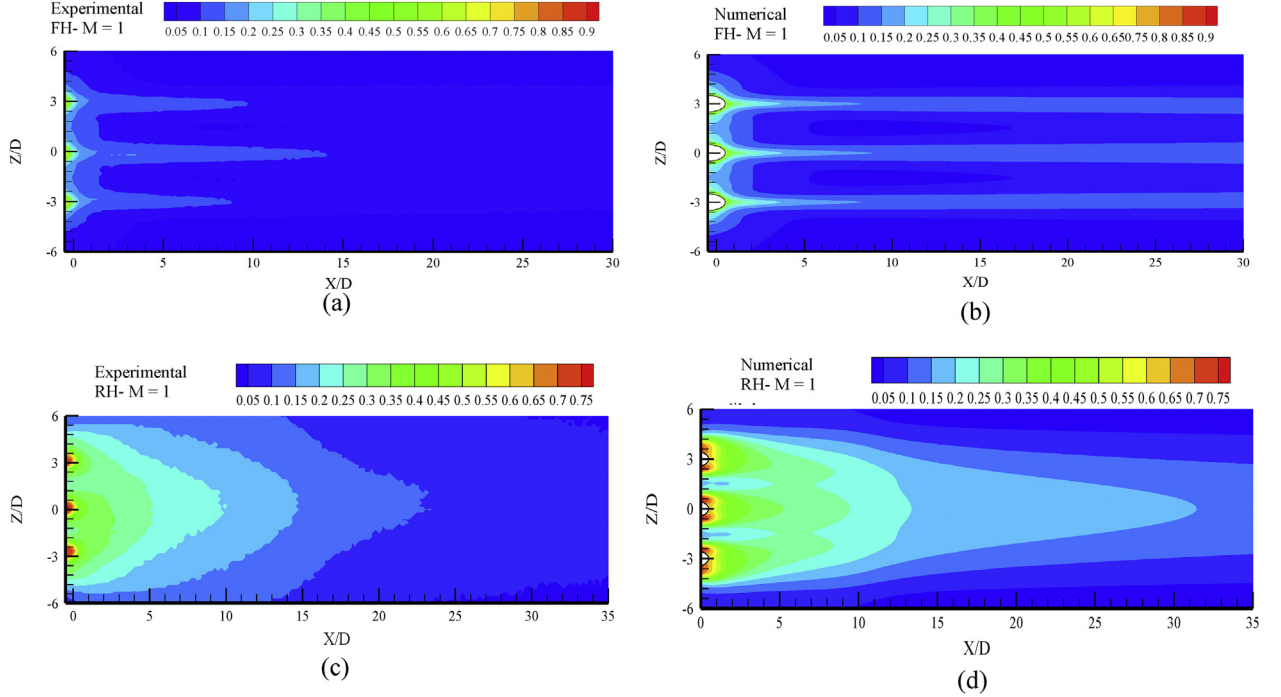


Fig. 7. Comparison of film cooling contours obtained from experimental and numerical studies (a) experimental forward holes (FH), $\alpha = 30^\circ$ (b) numerical FH, $\alpha = 30^\circ$ (c) experimental reverse hole (RH), $\alpha = 30^\circ$ (d) numerical RH, $\alpha = 30^\circ$.

et al. [30]. The numerical predictions of film cooling using the Realizable $k-\epsilon$ model are closer to the experimental results of Sinha

et al. [1] compared to that of other turbulent models. Hence, turbulence model Realizable $k-\epsilon$ is selected for parametric studies.

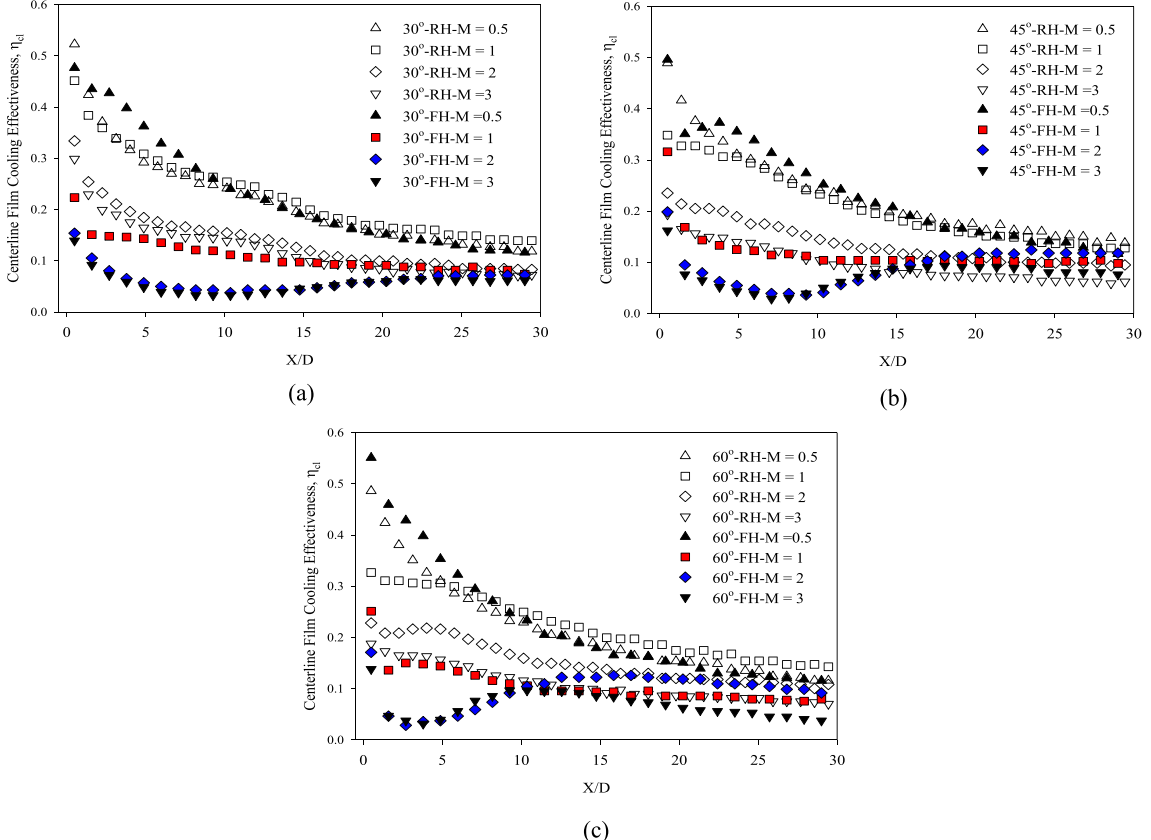


Fig. 8. Variation of centerline film cooling effectiveness with the investigated blowing ratios for (a) 30° forward and reverse holes (b) 45° forward and reverse holes (c) 60° forward and reverse holes.

The results obtained from the experimental and numerical studies on film heating for forward and reverse holes inclined at an angle, $\alpha = 30^\circ$ at $M = 1$ and mainstream Reynolds number, $Re = 3.75 \times 10^5$ are shown in Fig. 6. It can be seen from this figure that the centerline film heating effectiveness obtained from the experimental results are lower than that obtained from the numerical results. The difference between the numerical results and experimental results is higher near the film heating hole, and gradually decreases with increase in downstream distance. The average difference in the centerline film cooling effectiveness obtained from the experimental and numerical studies is approximately 22%. The corresponding difference in the predicted and measured surface temperature is 6.5°C . The estimated uncertainty in experimental measurement of temperature is 4°C . Thus we may say that the numerical prediction is very close to the experimental results. The qualitative analysis of film heating effectiveness by forward and reverse holes can be seen from the contours plots in Fig. 7. Although there is slight difference in the spread of secondary fluid on test plate obtained from the numerical and experimental studies, the numerical results look qualitatively similar and quantitatively close to the experimental results.

Hence, it can be concluded that the numerical model and the procedure adopted in the current work are capable of predicting film heating effectiveness reasonably closely.

4. Results and discussion

A detailed experimental study is carried out to compare the film cooling performance of forward injection holes and reverse injection holes. Experiments are conducted for five blowing ratios (M) ranging from 0.25 to 3.0. The injection angle is varied from 30° to

60° with respect to the flat surface in both forward and backward direction. The length-to-diameter ratio of the holes, L/D is kept at 5 and the mainstream Reynolds number is maintained at 3.75×10^5 . The flow visualization and pressure drop calculations are carried out with the help of numerical analysis. The numerical results are also presented for blowing ratio ranging from 0.25 to 3.0.

In the present study both experimental and numerical studies are carried out at a density ratio, $DR = 0.91$. A density ratio less than 1.0 indicates that the temperature of injected fluid is more than mainstream fluid. Singh et al. [31] showed that film heating is analogous to film cooling when density ratio is close to unity. Hence, in the present work ‘film cooling’ is used in the discussion instead of film heating.

4.1. Centerline film cooling effectiveness

The variation of centerline film cooling effectiveness for blowing ratio ranging from $M = 0.5$ – 3 is shown in Fig. 8 for both forward and reverse holes. It can be seen from the figure that the centerline film cooling effectiveness obtained from forward hole for blowing ratio $M = 0.5$ is comparable with that of reverse hole at all the injection angles. At the higher blowing ratio, the centerline film cooling effectiveness obtained from the reverse holes is much higher than that from forward holes for all the investigated injection angles. It can also be observed that the centerline film cooling effectiveness for the forward injection holes drop down to a lower value just after the injection hole and after a certain downstream distance it increases for higher blowing ratios. This is the indication of the secondary jet lift off and reattachment. Such a trend is not followed by reverse hole injection. In case of the forward injection holes, it is well known that the secondary fluid jet issued from

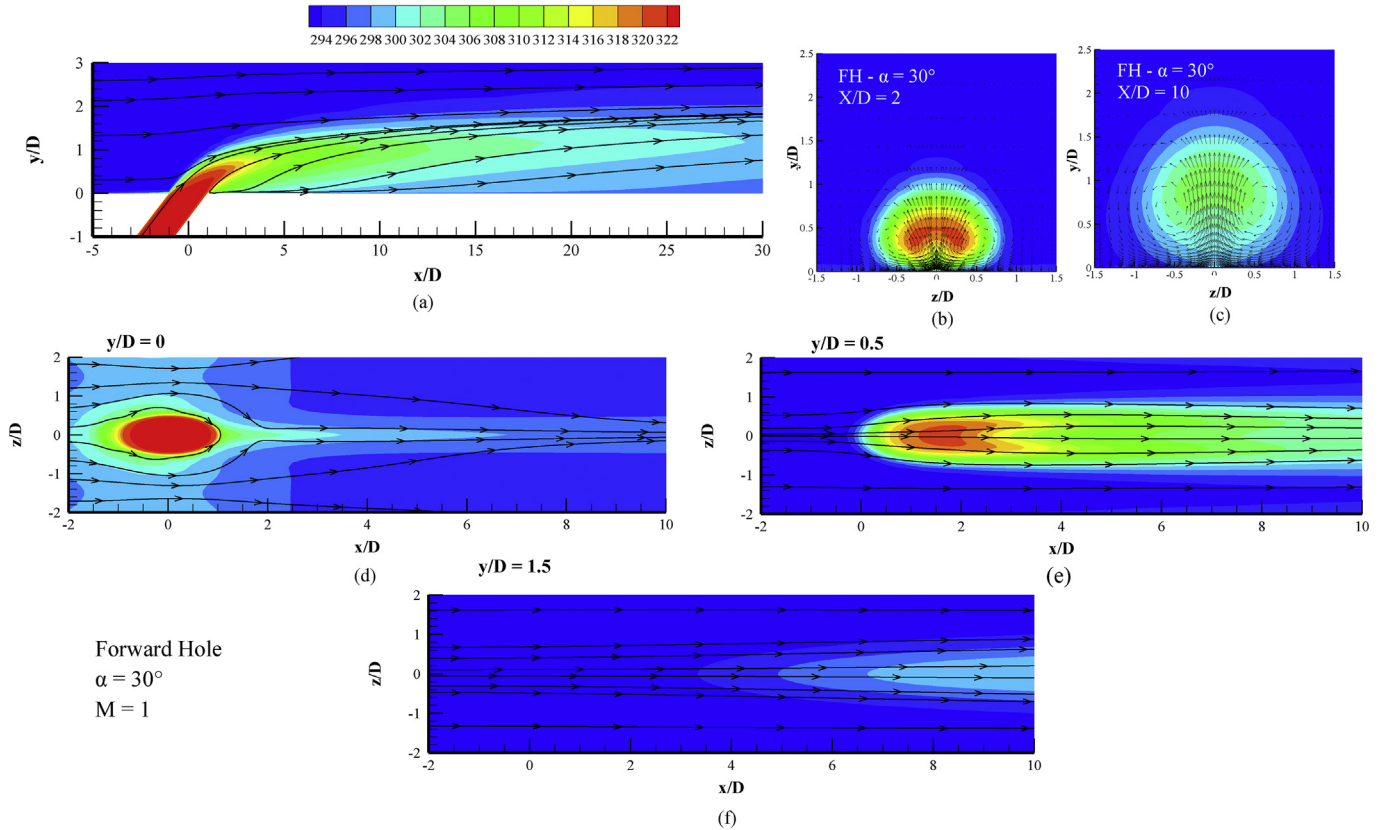


Fig. 9. Streamlines colored by temperature downstream for forward cooling holes at blowing ratio, $M = 1$ and injection angle, $\alpha = 30^\circ$ (a) front view, (b & c) side views at $x/D = 2$ and 10 respectively, (d, e, f) top view at $y/D = 0, 0.5$ and 1.5 respectively.

simple cylindrical holes forms kidney vortices [4] which diminishes the film cooling effectiveness.

The flow structure downstream of the cooling holes provides insight into the mechanism of film cooling in the case of forward and reverse holes. Fig. 9 shows the streamlines colored by temperature value, in the region downstream of the cooling hole in the case of forward holes. Fig. 9(a) shows flow in the X-Y plane through the centerline of central hole. It is clearly seen from Fig. 9 (a) that the secondary fluid penetrates into the mainstream and bends in the direction of the flow because of the impact of the mainstream. Fig. 9 (b & c) show the velocity vectors in the Y-Z plane i.e. the plane perpendicular to the direction of flow. Formation of the kidney vortices is captured in Fig. 9 (b). It can be observed that the jet of secondary air splits into two counter-rotating vortices. It can also be observed from Fig. 9 (b) that the secondary fluid is slightly lifted off from the target surface. The jet lift-off and size of the kidney vortices increase with the increase in downstream distance as depicted in Fig. 9 (c). These observations are consistent with the findings in the literature: Fric and Roshko [2] showed that the kidney-vortices are formed in the near-field region of hole, which grow as the flow moves downstream of the holes and dominate in the far field region. The spread of secondary fluid on the plane of the test plate i.e. X-Z plane at different horizontal planes above the target surface is shown in Fig. 9 (d–f). The location $y/D = 0$ is the surface of test plate. In order to show stream lines, temperature contours are plotted one grid point above the surface of test plate. It can be seen from Fig. 9 (d) that the spread of secondary fluid is confined to a very narrow region along the centerline. Traces of the mainstream air can be seen on the surface just downstream of the cooling hole i.e. at $x/D = 1$. This indicates that the mainstream air

remains entrapped below the trajectory of the secondary fluid. Distribution of the secondary air on a plane parallel to the test plate situated at $y/D = 0.5$ is more uniform. This indicates that the injected secondary fluid is being wasted without fulfilling the objective of the cooling of target surface. On a plane parallel to test plate situated at $y/D = 1.5$, most of the secondary fluid is washed away near the cooling hole as shown in Fig. 9 (f).

Flow structures in the case of reverse injection holes are found entirely different from that of observed with forward holes as can be seen in Fig. 10. In the case of reverse hole, the secondary air turns back and aligns itself to the flow direction due to the impact of mainstream air as evident from Fig. 10 (a). The velocity vectors on a plane perpendicular to the direction of flow (Y-Z) indicate the absence of kidney vortices in the case of reverse holes as shown in Fig. 10 (b & c).

In the case of reverse hole, formation of vortices can be observed on horizontal planes parallel to the flow direction (X-Z plane) as shown in Fig. 10 d & e. The velocity components in these vortices do not have the tendency to lift-off from the surface. Presence of these vortices enhances the mixing with the mainstream fluid. But, the secondary fluid remains close to the wall. Also the spread of the secondary fluid increases in the lateral direction as seen in Fig. 10 d. The comparison of Fig. 9 (d) and Fig. 10 (d) shows the merit of injection of secondary fluid from reverse holes. The upward momentum of kidney vortices in the case of forward injection holes leads to the mixing of secondary fluid with the mainstream far away from the surface. In contrast, in the case of reverse holes, the secondary fluid mixes with the mainstream and it remains close to the wall. The comparison of Fig. 10d and (e and f) also reveals that the vortices formed in the case of reverse hole are diminished as the

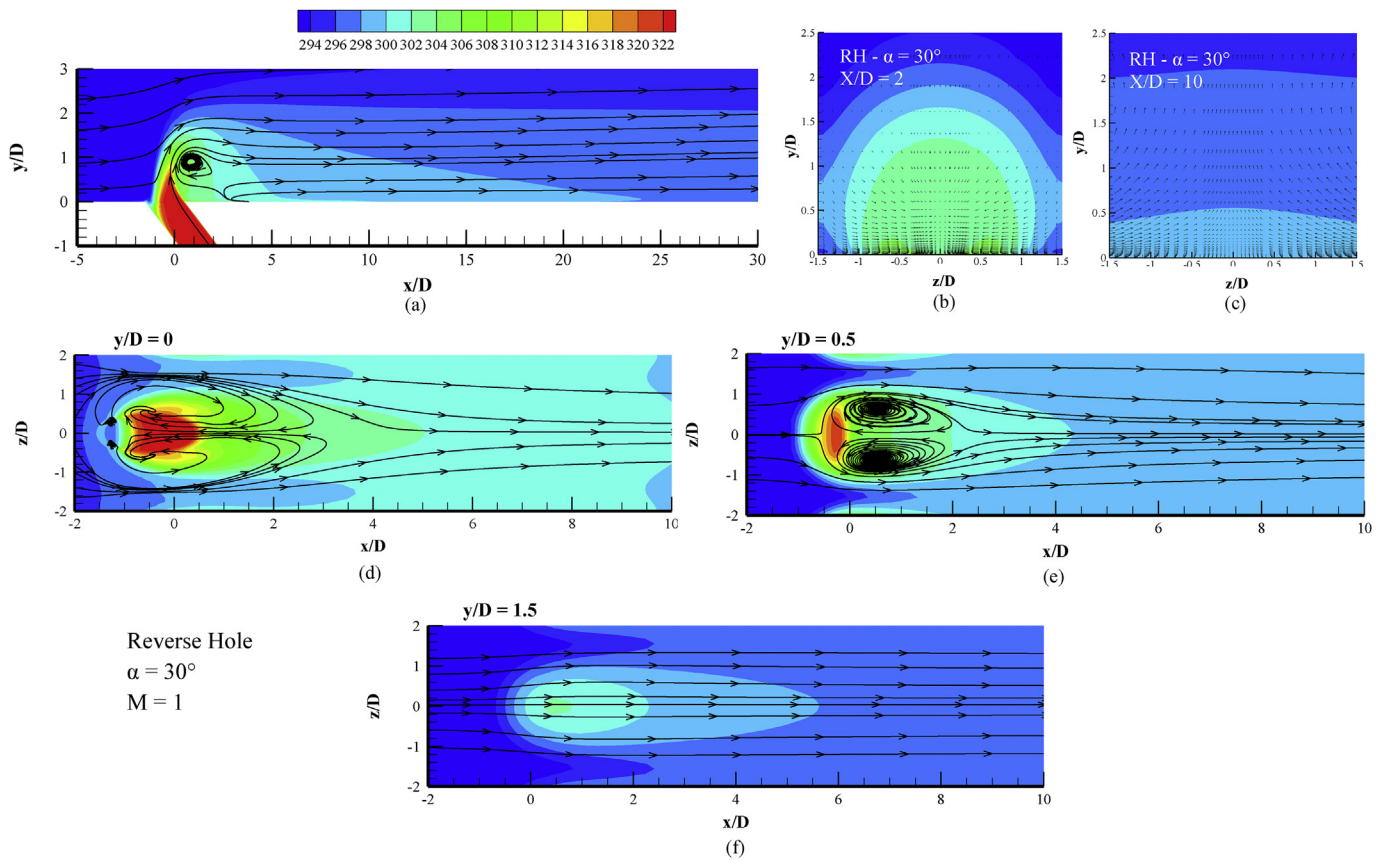


Fig. 10. Streamlines colored by temperature downstream for reverse holes at blowing ratio, $M = 1$ and injection angle, $\alpha = 30^\circ$ (a) front view, (b & c) side views at $x/D = 2$ and 10 respectively, (d, e, f) top view at $y/D = 0, 0.5$ and 1.5 respectively.

distance in the vertical direction increases from $y/D = 0$ to $y/D = 1.5$.

From the flow features it can be seen that the spread of the secondary fluid over the surface in the case of reverse hole is much better as compared to the case of forward hole. Hence, improvement in film cooling effectiveness is observed.

4.2. Lateral variation of local film cooling effectiveness

The lateral variation of local film cooling effectiveness at downstream distances, $X/D = 5$ and $X/D = 10$ is shown in Fig. 11 for the forward and the reverse holes for the injection angles, $\alpha = 30^\circ$ and 60° and the blowing ratios, $M = 1$ and 2 . It can be seen from Fig. 11 that for the forward holes, the spread of the secondary fluid is skewed towards the centerline of cooling holes, particularly at the blowing ratio, $M = 1$. The spread of secondary fluid in between the cooling holes is poor, which leads a drop in cooling effectiveness and hence, rises temperature in this region. In order to cool the surface adequately with the forward injection holes, either the pitch of the cooling holes has to be decreased or more rows of cooling holes have to be made in a staggered pattern. For the forward injection holes at the blowing ratio, $M = 1$, it can be seen that the spread of secondary fluid is almost uniform (Fig. 12 a–c) but effectiveness is very low. This is because of the lift-off of the secondary fluid. Film cooling effectiveness improves as jet of secondary fluid reattaches with the surfaces as can be seen in Fig. 11d for $\alpha = 60^\circ$ and $M = 1$. On the contrary, reverse holes provide almost

uniform spread of the secondary fluid in the lateral direction. Since in the present experiments only single row of three cooling holes are present, the effectiveness is highest at the central hole and it tapers off slightly towards the side holes. But it can be seen that the variation is not significant. The uniform spread in between the cooling holes ensures no hot patches and improves the cooling effectiveness. This is evident from the contours plots shown in Fig. 12. From these plots it can be seen that the region between the cooling holes is not cooled adequately in case of forward holes. For the forward holes, the spread of secondary fluid is restricted to a lateral distance of the size of cooling holes. Even within this narrow region covered by the secondary fluid film, the centerline film cooling effectiveness obtained from forward holes is lower as compared to that from reverse holes for same blowing ratio. This indicates that the mixing of the secondary fluid with the mainstream fluid is more for the forward holes as compared to the reverse holes, leading to less effective protection of the surface from hot secondary steam.

4.3. Lateral average film cooling effectiveness

The variation of lateral average film cooling effectiveness for blowing ratio ranging from $M = 0.5$ – 3 is shown in Fig. 13 for both forward and reverse holes. The lateral average was taken over a distance $-4D$ to $4D$ from the central hole. The lateral average film cooling effectiveness thus represents the coverage of secondary fluid film at each streamwise location downstream of the injection

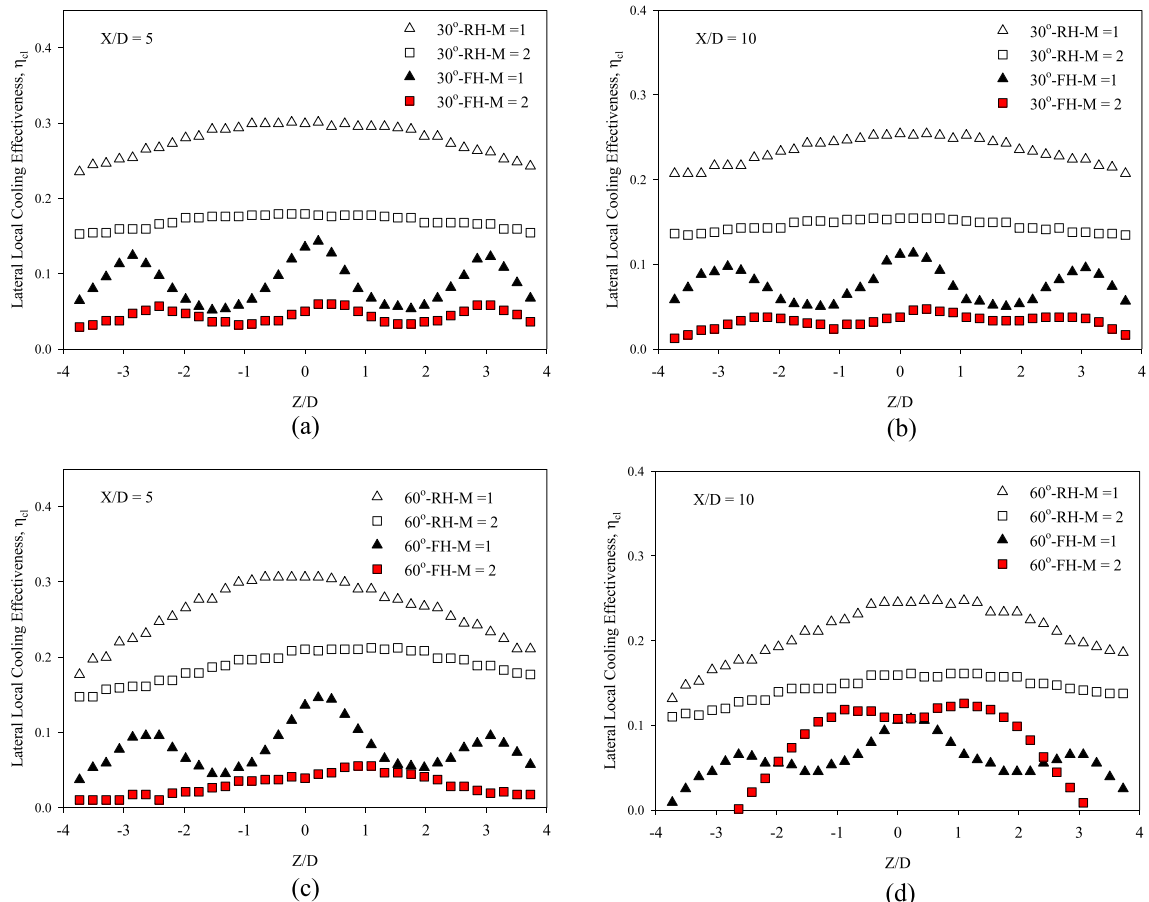


Fig. 11. Variation of lateral local film cooling effectiveness for blowing ratios, $M = 1$ and 2 and 10 , (a) 30° forward and reverse holes at downstream locations $X/D = 5$, (b) 30° forward and reverse holes at downstream locations $X/D = 10$, (c) 60° forward and reverse holes at downstream locations $X/D = 5$, (d) 60° forward and reverse holes at downstream locations $X/D = 10$.

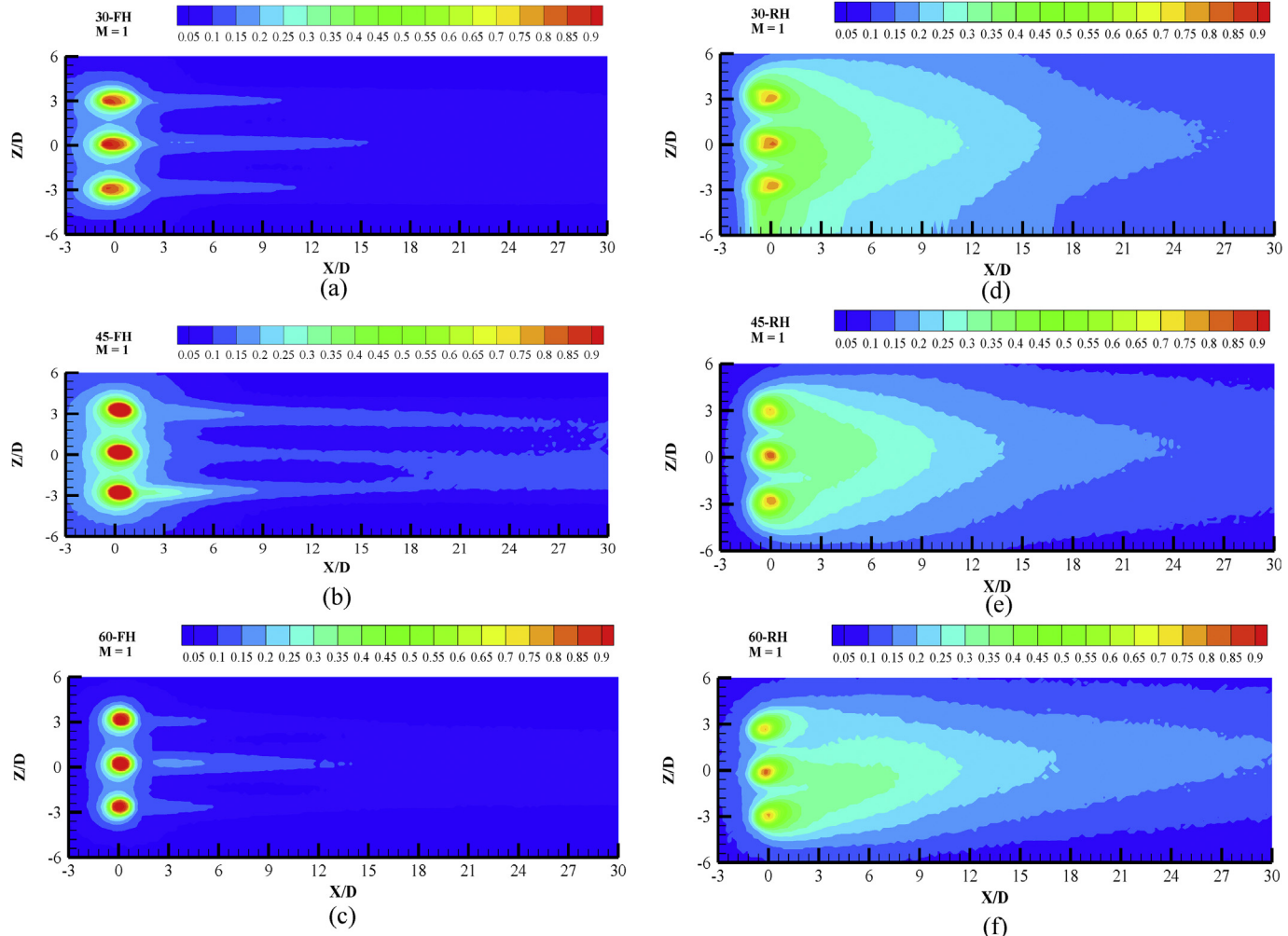


Fig. 12. Film cooling effectiveness contours for blowing ratio, $M = 1$ (a) 30° forward hole (b) 30° reverse hole (c) 45° forward hole (d) 45° reverse hole (e) 60° forward hole (f) 60° reverse hole.

holes. It can be seen from Fig. 13 that the reverse injection holes exhibits much better lateral average film cooling effectiveness as compared to the forward holes at all locations and at all the blowing ratios and the injection angles. The improvement in lateral film cooling effectiveness gets better as the blowing ratio increases. The reason for this trend can be understood with the help of the trends in lateral local film cooling effectiveness discussed in the Section 4.2. Since the film from reverse injection holes covers the surface more effectively than that from the forward holes, the lateral average at each location reflects this trend in Fig. 13 as well.

4.4. Effect of blowing ratio

The effect of blowing ratio on overall average film cooling effectiveness obtained from forward and reverse injection is shown in Fig. 14. The overall average film cooling effectiveness is computed over the region from $-4D$ to $4D$ in the lateral direction and 0 to $30D$ in the flow direction for all the cases investigated in the present study. It can be observed from Fig. 14 that at the lowest blowing ratio, the net gain in the film cooling effectiveness in the case of the reverse injection is lowest. The increment in area-weighted average film cooling effectiveness because of reverse injection is 4% for 30° , -2% for 45° and 57.5% for 60° at $M = 0.25$. This is because at lower blowing ratio the secondary fluid is not having sufficient

momentum to penetrate into the mainstream fluid. Hence, secondary fluid remains close to the surface. For higher blowing ratios i.e. for $M = 1$, the increment in the area-weighted average is 170%, 78% and 186%, for $M = 2$, the increment is 170%, 91.5% and 187%, for $M = 3$, the increment is 190%, 97% and 220% for injection angles $\alpha = 30^\circ, 45^\circ$ and 60° , respectively. The improvement in film cooling effectiveness at higher blowing ratios is due to difference in the film cooling mechanism. The mechanism responsible for improvement in film cooling effectiveness is already explained in Section 4.1.

4.5. Effect of injection angle

The variation of lateral average film cooling effectiveness at blowing ratios, $M = 1$ and $M = 2$ is shown with the investigated injection angles in Fig. 15. It can be seen from this figure that the injection angle does not exhibit monotonic increment or decrement in the film cooling effectiveness at any location downstream of the injection hole; the lines are seen to cross each other at one or more locations in Fig. 15 a and b, for both forward and reverse injections. But the change in film cooling effectiveness with injection angle in cases of reverse injection is observed to be smaller in magnitude compared to corresponding cases of forward injection. At a downstream distance of $X/D = 10$, the difference between highest and lowest values of film cooling effectiveness is 13% for

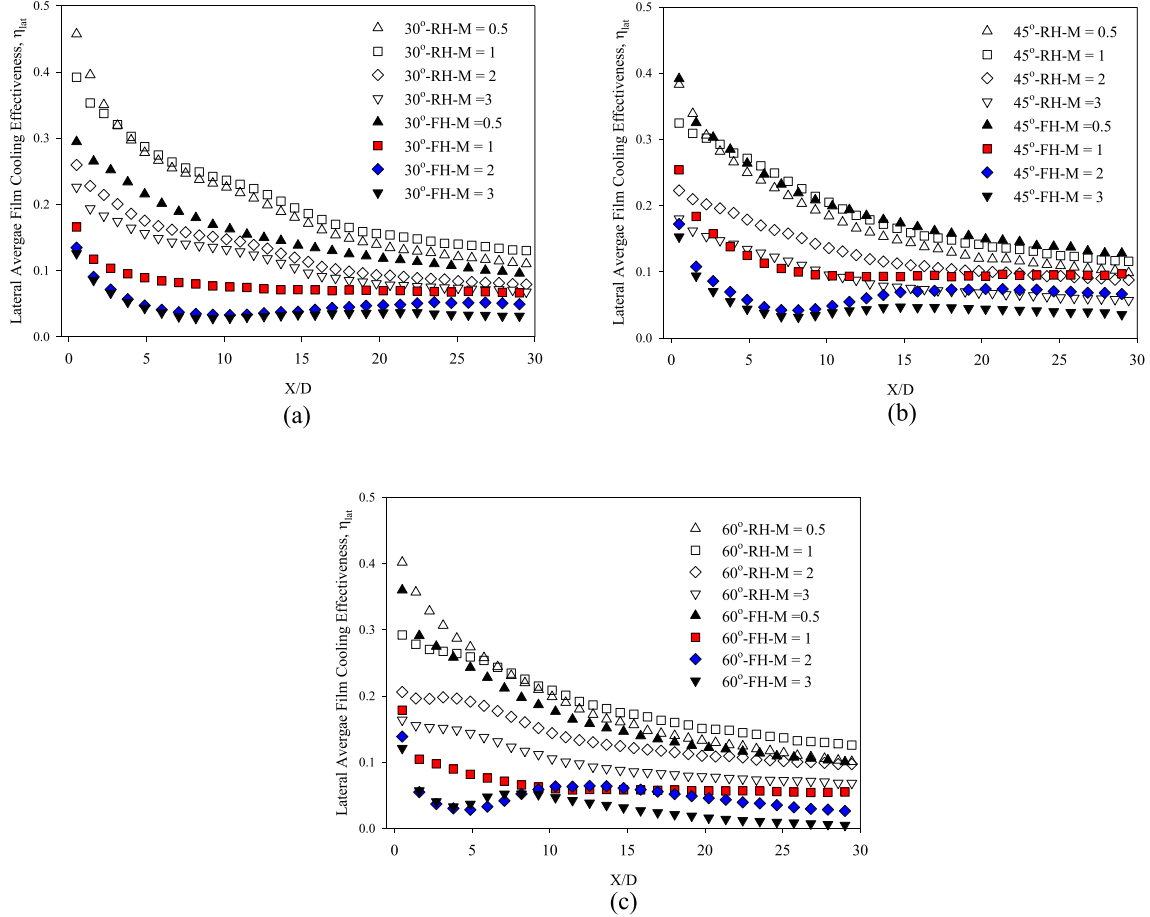


Fig. 13. Variation of lateral average film cooling effectiveness with the investigated blowing ratios for (a) 30° forward and reverse holes (b) 45° forward and reverse holes (c) 60° forward and reverse holes.

reverse holes and 36% for forward holes. This indicates that the reverse holes are less sensitive to change in injection angle as compared to the forward holes. It is because the lift off of secondary fluid ejected from forward holes depends strongly on angle of injection but that from reverse holes is turned back due to the impact of the mainstream and uniformly spreads over the surface without being lifted-off as can be observed from Fig. 16. This mechanism is already discussed in detail in the Section 4.1.

4.6. Effect of density ratio

The effect of density ratio is investigated by varying density ratio in the range of 0.91–2.5 at a fixed blowing ratio, $M = 1$ for both forward and reverse injection holes inclined at an angle 30° to the test plate. Film cooling effectiveness contours downstream of the cooling holes are shown in Fig. 17 for both forward and reverse injection angle. It can be seen from this Fig. 17 (a–c) that film cooling coverage of the secondary fluid increases as density ratio increases from 0.91 to 2.5 for forward hole. For a fixed blowing ratio, increase in density ratio results in decrease in the injection velocity for a given mainstream Reynolds number. This reduces the penetration of the secondary fluid into mainstream and hence formation of kidney vortices is suppressed upto some extent. Eventually, film cooling effectiveness increases with the increase in density ratio. It can also be seen from Fig. 17 (d–f) that the lateral spread of secondary fluid decreases as density ratio increases for reverse injection. But, the coverage of secondary fluid is better for

reverse injection as compared to forward injection at all the investigated density ratios.

Lateral spreading of the secondary fluid in the case of reverse injection is because of formation of vortices in the plane of test plate i.e. X-Z plane as explained in Section 4.1. At higher density ratio, the formation of vortices in the plane of the test plate is also suppressed as can be seen by streamline traces in Fig. 17 (d–f) and hence lateral spreading.

4.7. Discharge coefficient (C_d)

It was observed in the previous section that the film cooling performance of reverse holes is much better than forward holes. However, one might expect that since in reverse injection the secondary flow has to be pushed in the direction opposite to the mainstream, it may involve higher pressure losses and demand a higher pumping power. In order to investigate pressure losses, discharge coefficients of the investigated film cooling holes is presented.

The discharge coefficient of the film cooling hole is a measure of pressure losses in the cooling holes. It can be defined as the ratio of actual mass to the ideal mass flow through the film cooling hole, for a specified pressure ratio across the hole.

$$C_d = \frac{(m_c)_{actual}}{(m_c)_{ideal}} \quad (3)$$

The ideal mass flow rate is calculated using eq. (4), assuming

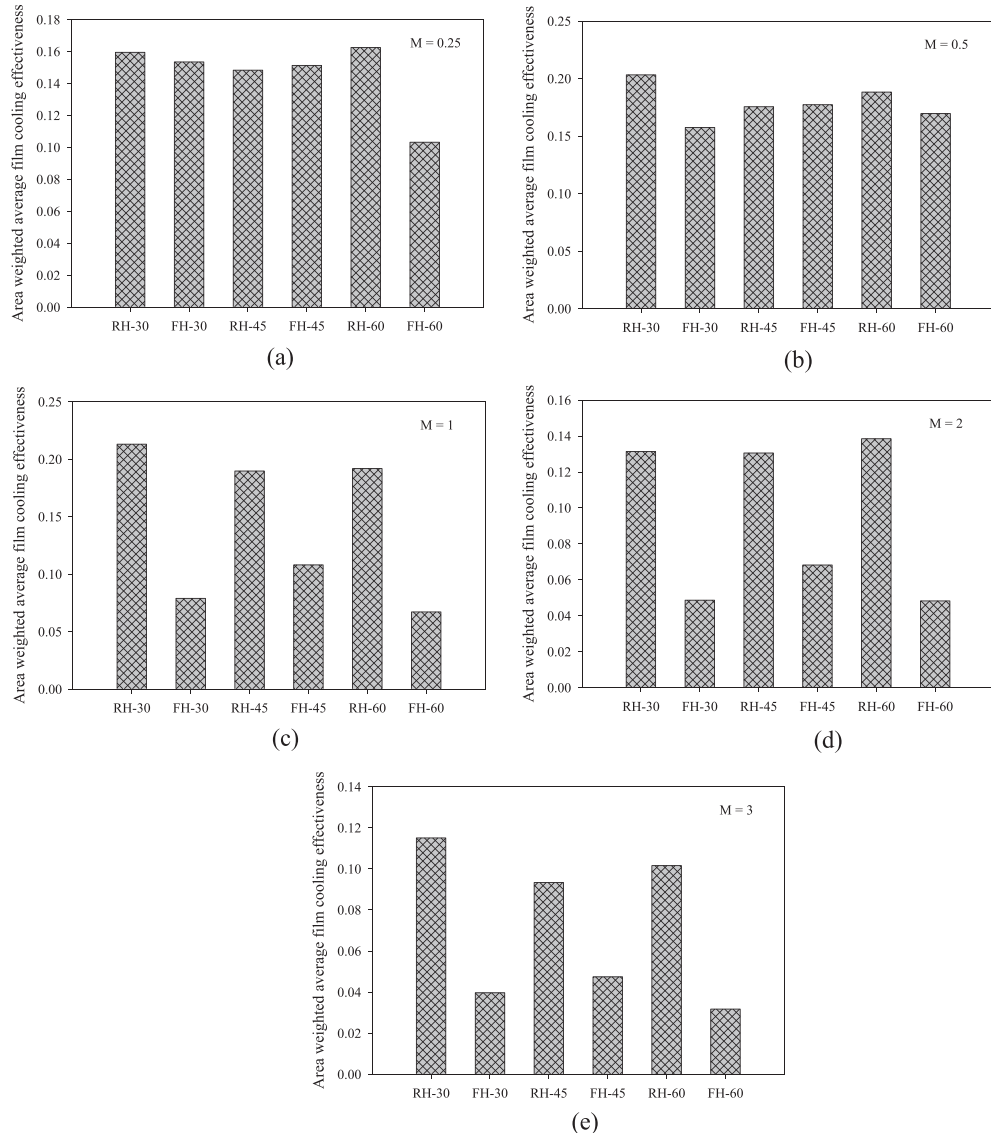


Fig. 14. Comparison of area weighted average film cooling effectiveness for all the investigated blowing ratios and injection angles.

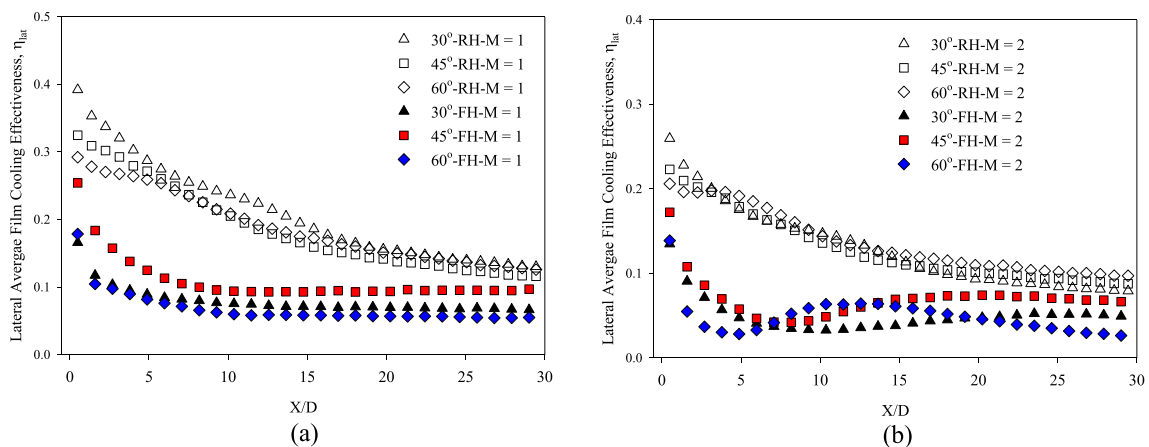


Fig. 15. Comparison of effect of injection angle (forward and reverse) on film cooling effectiveness at blowing ratios, $M = 1$ and $M = 2$.

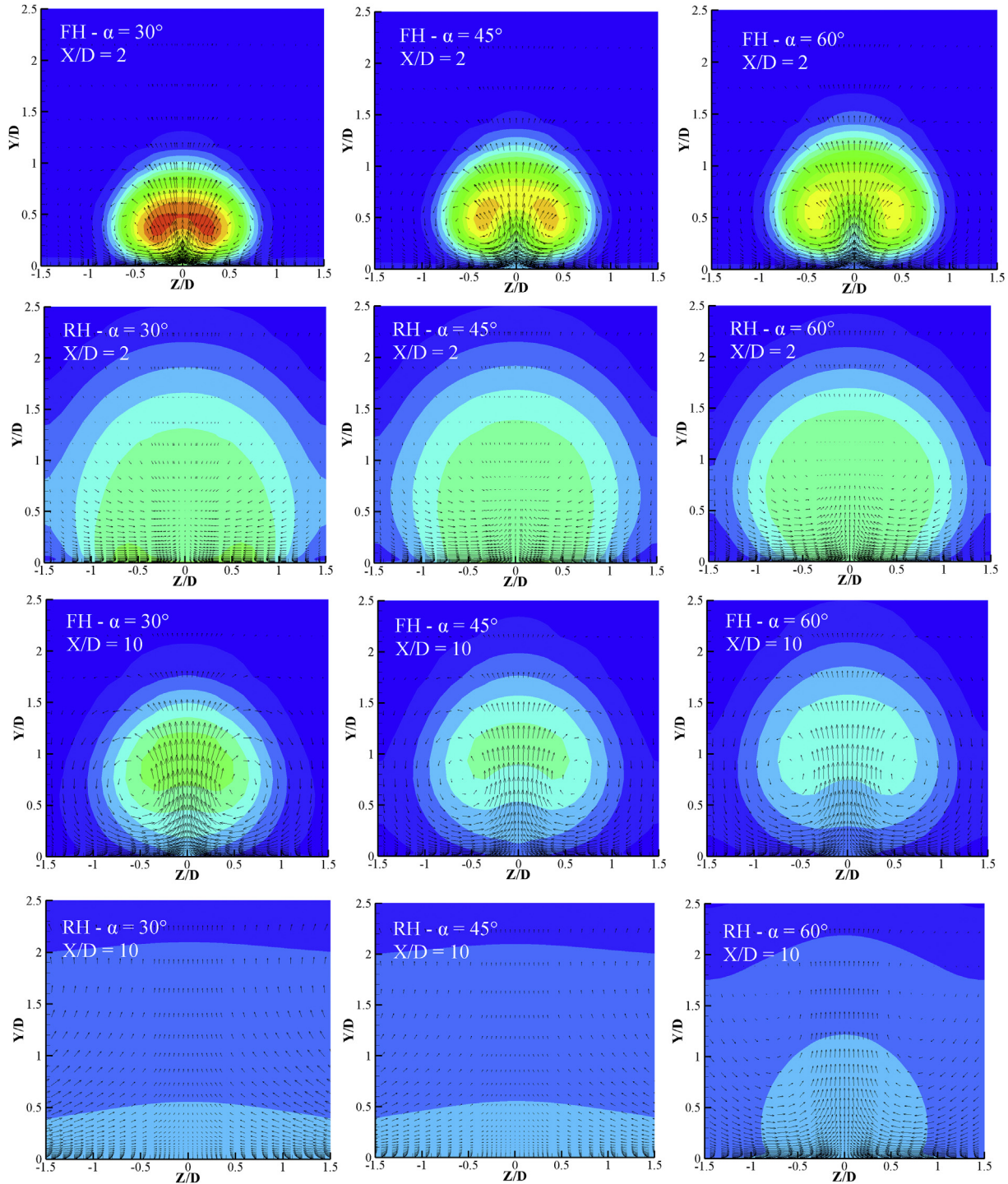


Fig. 16. Velocity vectors superimposed on temperature contours on the planes perpendicular to the mainstream direction ($X/D = 2$ and $X/D = 10$) for forward and reverse holes.

isentropic, one-dimensional expansion across the cooling hole from coolant total pressure ($p_{t,c}$) to the main flow static pressure (p_m) level.

$$m_{\text{ideal}} = A_c p_{t,c} \left(\frac{p_m}{p_{t,c}} \right)^{\lambda+1/2\gamma} \sqrt{\frac{2\gamma}{(\gamma-1)RT_{t,c}}} \left[\left(\frac{p_{t,c}}{p_m} \right)^{\gamma-1/\gamma} - 1 \right] \quad (4)$$

where A_c is the cross sectional area of cylindrical cooling hole, γ is the ratio of specific heats, R is the gas constant, $T_{t,c}$ is the coolant total temperature.

Total pressure was taken at the entrance (plenum side) of the cooling and p_m is taken $X/D = -5$ i.e. upstream of the cooling holes hole as described by Taslim and Ugarte [35]. This has now been clarified in the text of the paper as well. Symbol for specific heat ratio has also been corrected.

The variation of C_d with the investigated injection angles is

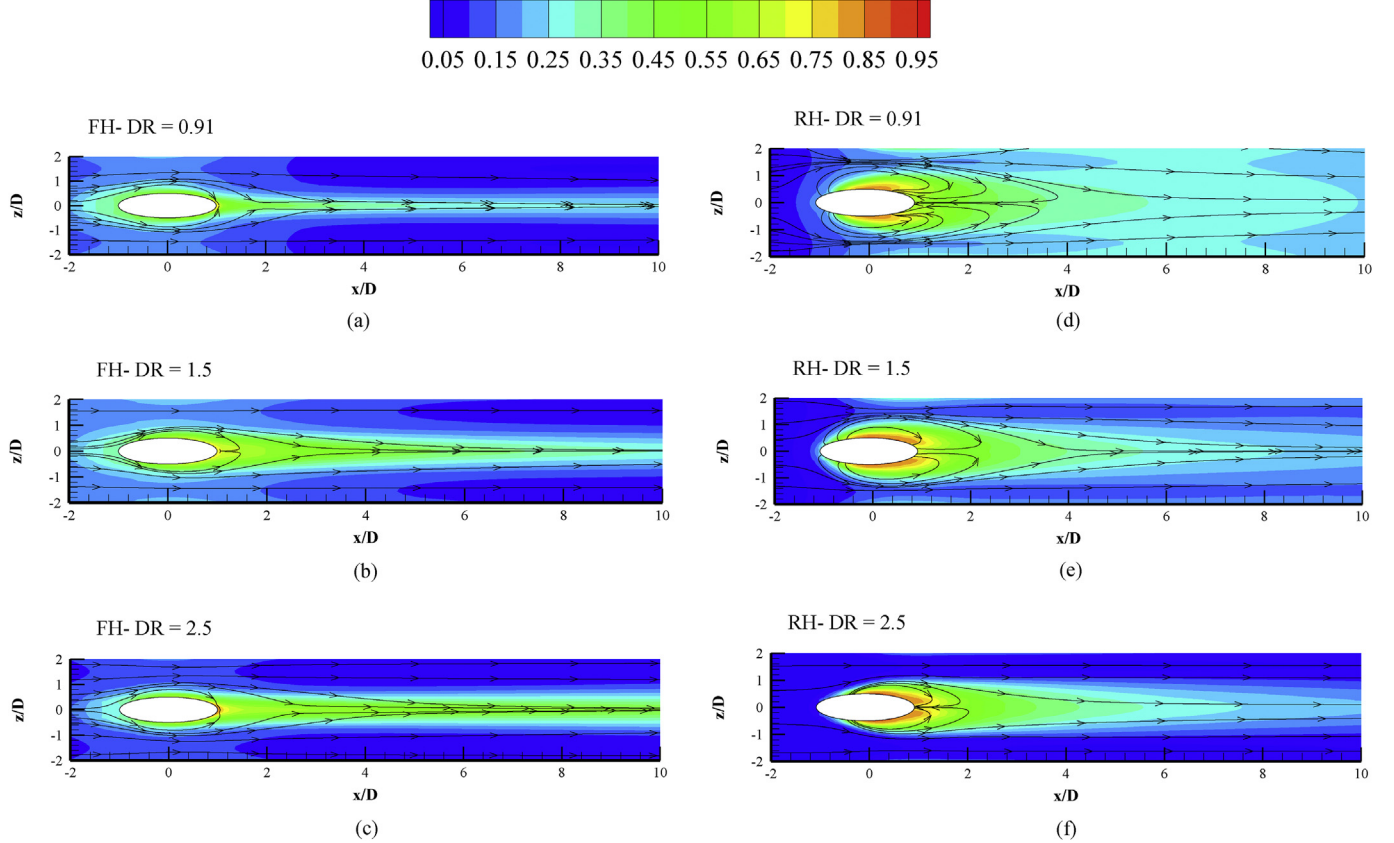


Fig. 17. Film cooling effectiveness contours along with streamlines for blowing ratio, $M = 1$, injection angle 30° (a) DR = 0.91, forward hole (b) DR = 1.5, forward hole (c) DR = 2.5, forward hole (d) DR = 0.91, reverse hole (e) DR = 1.5, reverse hole (f) DR = 0.91, reverse hole.

shown in Fig. 18 for the blowing ratio, $M = 1$. In this figure the values of discharge coefficient obtained from the present study are also compared with the results of Yao et al. [32] for the forward hole inclined at 30° and with Guangchao et al. [33] for the forward hole inclined at 45° at a blowing ratio, $M = 1$. The present results are comparable with the results of Yao et al. [32] and Guangchao et al. [33]. The deviation in the values of discharge coefficient is 2.3% from Yao et al. and 4.68% from Guangchao et al. which may be attributed to the difference in the lengths of film cooling holes and

the velocity of mainstream. The discharge coefficient of the branched holes was investigated by Yao et al. [32], Li et al. [34] and conical holes studied by Taslim and Ugarte [35] are also presented in Fig. 18 for quantitative comparison. The value of discharge coefficients of these studies lie in between the discharge coefficient of forward and reverse holes.

Fig. 18 reveals that the discharge coefficient of the forward holes is higher than the reverse holes for all the investigated injection angles. The discharge coefficient of forward hole inclined at 30° is 21% higher as compared to reverse hole inclined at 30° which drops down to 12% and 13% for 45° and 60° injection angles, respectively. It can also be seen from this figure that the discharge coefficient is strongly influenced by the angle of injection. It increases as the injection angle increases for both types of the holes i.e. forward inclined and reverse inclined. The discharge coefficient is inversely proportional to the pressure drop in the cooling hole. Hence, it can be concluded that pressure loss in case of reverse holes is more as compared to the forward holes.

Fig. 19 shows the velocity contours at the exit of central hole for both the forward and reverse holes at 45° inclination angle. It can be observed that the velocity at the leading edge of the reverse hole is low. This is because of the interaction of the cross-flow with the secondary flow. Since, the reverse holes eject the secondary fluid in the opposite direction of the mainstream flow; the high momentum of the cross-flow suppresses the secondary fluid near the leading edge. This causes a partial blockage towards the leading edge which results in increase in the velocity at the trailing edge. Because of the partial blockage of the reverse cooling holes near leading edge, the coefficient of discharge is low for these holes. The velocity magnitude non-dimensionalized by mainstream velocity

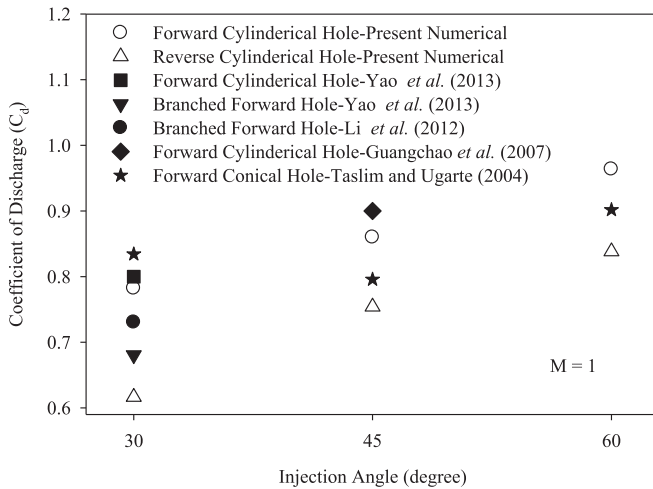


Fig. 18. Variation of coefficient of discharge with injection angle.

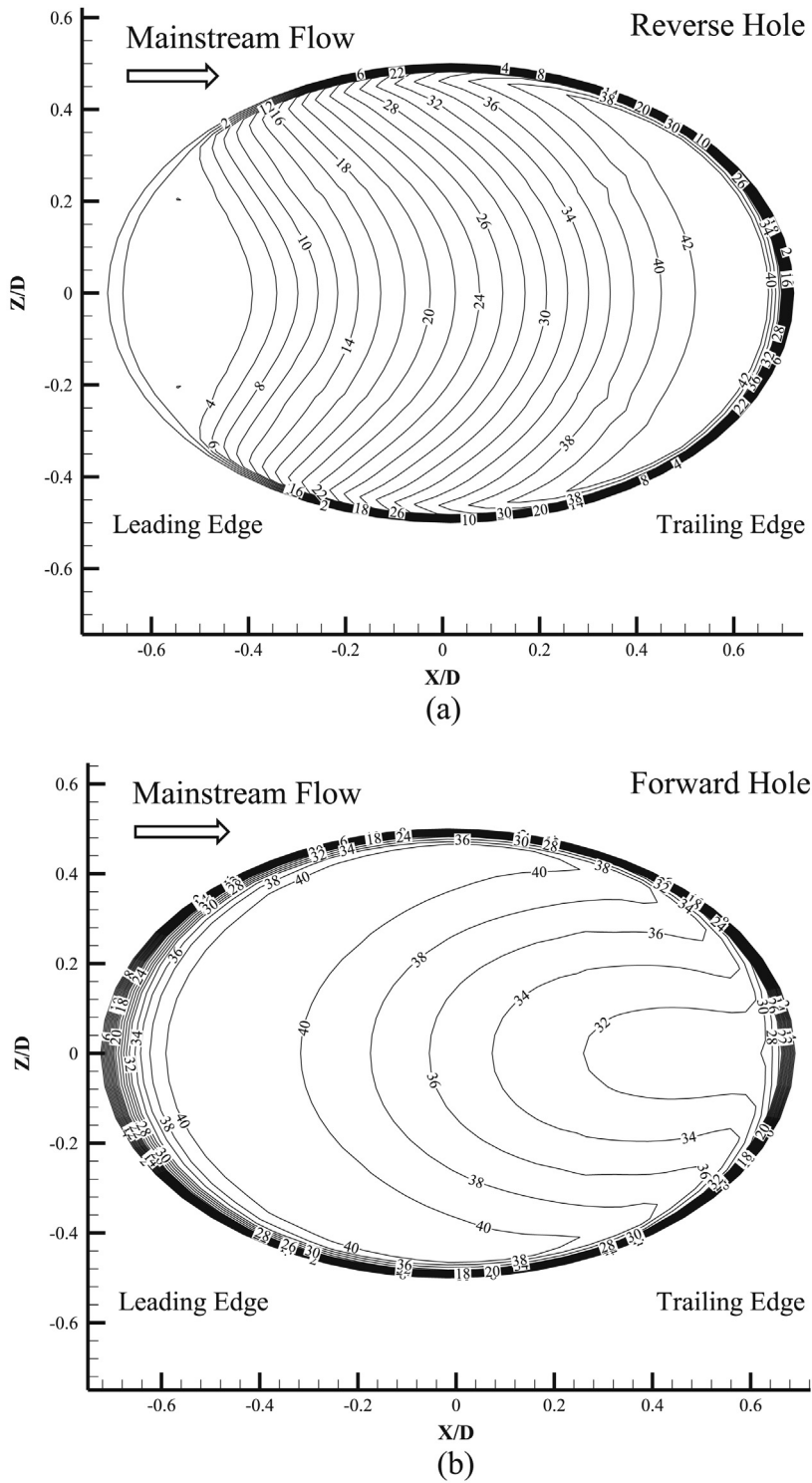


Fig. 19. Velocity contours at the exit of cooling hole for 45° injection angle at blowing ratio, $M = 1$ (a) Forward Hole (b) Reverse Hole.

at the cooling hole exit in the direction of mainstream flow and lateral direction is shown in Fig. 20 for both forward and reverse hole inclined at an angle 45° at a blowing ratio, $M = 1$. It can be observed that the velocity profile through these holes does not follow fully developed pipe flow profile. This is because the length-to-diameter ratio of cooling holes investigated in the study is $L/D = 5$, i.e. the L/D ratio found in most of the applications, which is

not sufficient for development of flow. The velocity profile of RH-45° is skewed (Fig. 20a) with the peak shifted towards the trailing edge of the hole while the velocity profile of FH-45° is flattened as compared to RH-45°. In the lateral direction, the velocity magnitude of FH-45° is significantly higher than RH-45°. Because of this behavior, in forward hole, the bulk of secondary flow stay closer to mainstream thus promoting more mixing between secondary fluid

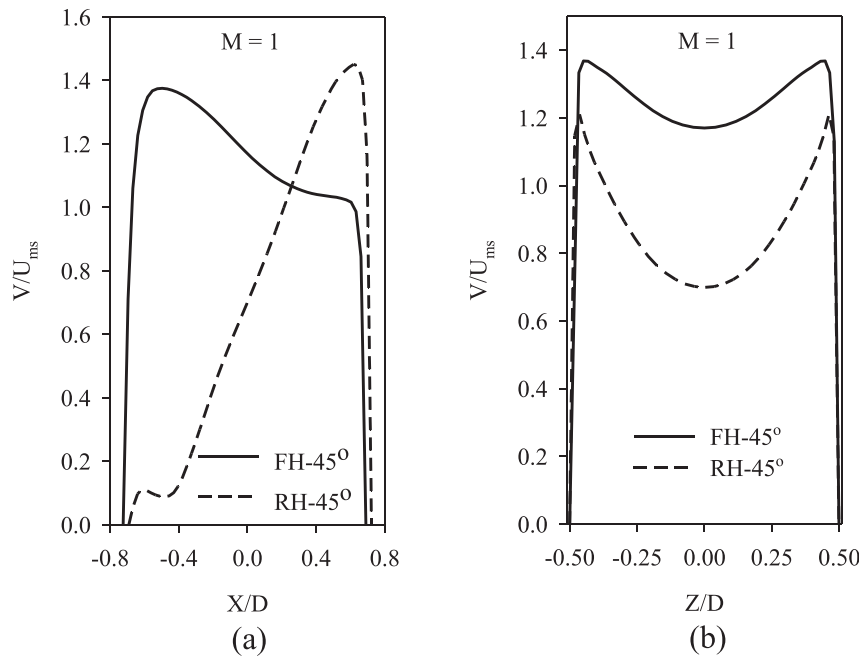


Fig. 20. Non dimensional velocity at the exit plane of cooling hole for 45° injection angle at blowing ratio, $M = 1$ (a) in direction of mainstream flow (b) in lateral direction.

and mainstream while in the reverse holes, bulk of the secondary flow stay closer to the surface and thus is more effective in spreading over the surface and improving the protection from the mainstream.

5. Conclusions

Film cooling performance of reverse holes has been investigated and it was compared with that of forward holes. The cooling hole injection angle was varied from 30° to 60° in both forward and backward direction at five blowing ratios ranging from 0.25 to 3 at a fixed density ratio of 0.91. Cooling hole length to the diameter ratio, L/D was kept 5 and mainstream Reynolds number was maintained 3.75×10^5 . The numerical study was carried out to visualize flow structure and to evaluate pressure losses in cooling holes. The numerical study was conducted at a fixed blowing ratio, $M = 1$, on all the injection angles for which experimental study was conducted. The followings points can be concluded from this study.

- Film cooling effectiveness obtained from reverse holes is much better than that of the forward holes at all the injection angles investigated in this study. At low blowing ratios i.e., $M = 0.25$ and 0.5 , the film cooling effectiveness of reverse holes is comparable with that of the forward holes. At higher blowing ratio the increase in film cooling effectiveness because of the reverse hole is 100%–220% compared to their counterpart, forward holes.
- Compared to the forward holes, the secondary fluid spreads more uniformly in the lateral direction in the case of reverse holes. The uniform spread on the lateral direction mitigates the hot patches which are found in the case of forward holes in between the cooling holes.
- The flow analysis indicates that kidney-vortices are evident in case of forward injection at all the injection angles. Kidney-vortices are not observed in the case of reverse holes and hence better film cooling is observed. Thus reverse holes provide a cost effective solution to suppress kidney vortices without adding to complexity in manufacturing.

- Pressure drop in the cooling hole is more in the case of reverse holes as compared to forward holes at a given blowing ratio and injection angle. However, the use of reverse hole would decrease the number of holes required to cool the system and hence net increase in the pumping work per unit mass of secondary fluid would be offset by smaller mass flow requirements. In addition to this, the problem of pressure drop can be resolved by suitable selection of injection angle. For example, instead of comparing FH-30° with RH-30°, one can select RH-60°. The comparison of RH-60° with FH-30° shows 144% improvement in film cooling effectiveness and 7.2% in discharge coefficient at blowing ratio, $M = 1$.

Overall, it can be concluded that the reverse holes have the potential to cool the hot surface more effectively. These holes are generally easy to manufacture, economic and suitable for thick as well as thin wall applications.

Acknowledgments

This research work was carried out under the research Grant, No. ERIP/ER/1000388/M/01/1298 sponsored by the Defence Research and Establishment Organization (DRDO), India.

References

- Irvine J, Thomas F, Hartnett JaP. *Advances in Heat Transfer*. seventh ed. New York: Academic Press; 1971.
- Fric TF, Roshko A. Vortical structure in the wake of a transverse jet. *J Fluid Mech* 1994;279:1–47. <http://dx.doi.org/10.1017/S0022112094003800>.
- Bidan GF. *Mechanistic Analysis and Reduced Order Modeling of Forced Film Cooling Flows*. Louisiana State University; 2013.
- Haven BA, Kurosaka M. Kidney and anti-kidney vortices in crossflow jets. *J Fluid Mech* 1997;352:27–64. <http://dx.doi.org/10.1017/S0022112097007271>.
- Goldstein RJ, Eckert ERG, Burggraf F. Effects of hole geometry and density on three-dimensional film cooling. *Int J Heat Mass Transf* 1974;17:595–607.
- Bunker RS. A review of shaped hole turbine film-cooling technology. *J Heat Transf* 2005;127:441–53. <http://dx.doi.org/10.1115/1.1860562>.
- Gritsch M, Schulz A, Wittig S. Adiabatic wall effectiveness measurements of

- film-cooling holes with expanded exits. *ASME J Turbomach* 1998;120: 549–56.
- [8] Bell CM, Hamakawa H, Ligrani PM. Film cooling from shaped holes. *J Heat Transf* 2000;122:224–32. <http://dx.doi.org/10.1115/1.521484>.
- [9] Saumweber C, Schulz A, Wittig S. Free-stream turbulence effects on film cooling with shaped holes. *J Turbomach* 2003;125:65–73. <http://dx.doi.org/10.1115/1.1515336>.
- [10] Silietti M, Kaasab AJ, Divo E. Film cooling effectiveness: comparison of adiabatic and conjugate heat transfer CFD models. *Int J Therm Sci* 2009;48:2237–48. <http://dx.doi.org/10.1016/j.ijthermalsci.2009.04.007>.
- [11] Cho HH, Rhee DH, Kim BG. Enhancement of film cooling performance using a shaped film cooling hole with compound angle injection. *JSME Int. J. Ser. B* 2001;44:99–110.
- [12] Yu Y, Yen C-H, Shih TI-P, Chyu MK, Gogineni S. Film cooling effectiveness and heat transfer coefficient distributions around diffusion shaped holes. *J Heat Transf* 2002;124:820–7. <http://dx.doi.org/10.1115/1.1418367>.
- [13] Taslim MEE, Khanucheh A. Film effectiveness downstream of a row of compound angle film holes. *J Heat Transf* 2005;127:434–40. <http://dx.doi.org/10.1115/1.1865222>.
- [14] Colban WF, Thole KA, Bogard D. A film-cooling correlation for shaped holes on a flat-plate surface. In: Proc. ASME Turbo Expo 2008 Power Land, Sea air; 2008. p. 1–15.
- [15] Lee KD, Kim KY. Shape optimization of a fan-shaped hole to enhance film-cooling effectiveness. *Int J Heat Mass Transf* 2010;53:2996–3005. <http://dx.doi.org/10.1016/j.ijheatmasstransfer.2010.03.032>.
- [16] Wright LM, McClain ST, Clemenson MD. Effect of density ratio on flat plate film cooling with shaped holes using PSP. *J Turbomach* 2011;133. <http://dx.doi.org/10.1115/1.4002988>. 041011–1 to 041011–11.
- [17] Dhungel A, Lu Y, Phillips W, Ekkad SV, Heidmann J. Film cooling from a row of holes supplemented with antivortex holes. *J Turbomach* 2009;131. <http://dx.doi.org/10.1115/1.2950059>. 021007–1–10.
- [18] Khajehhasani S, Jubran B a. Numerical assessment of the film cooling through novel sister-shaped single-hole schemes. *Numer Heat Transf Part A Appl* 2014;67:414–35. <http://dx.doi.org/10.1080/10407782.2014.937257>.
- [19] Lu Y. Effect of Hole Configurations on Film Cooling from Cylindrical Inclined Holes for the Application to Gas Turbine Blades. Louisiana State University; 2007.
- [20] Yang C, Zhang J. Experimental investigation on film cooling characteristics from a row of holes with ridge-shaped tabs. *Exp Therm Fluid Sci* 2012;37: 113–20. <http://dx.doi.org/10.1016/j.expthermflusci.2011.10.011>.
- [21] Li XC, Subbuswamy G, Zhou J. Performance of gas turbine film cooling with backward injection. *Energy Power Eng* 2013;05:132–7. <http://dx.doi.org/10.4236/epe.2013.54B025>.
- [22] Li S, Chen AF, Wang W, Han J. Experimental and computational film cooling with backward injection for cylindrical and fan-shaped holes. In: Proceedings 15th Int. Heat Transf. Conf. IHTC-15; 2014. p. 1–15.
- [23] Shetty S, Li X, Subbuswamy G. Numerical simulation on gas turbine film cooling of curved surface with backward injection. In: Proc. ASME 2012 Summer Heat Transf. Conf. HT2012, Rio Gd; 2012. p. 1–8.
- [24] Park S, Jung EY, Kim SH, Sohn H, Cho H. Enhancement of film cooling effectiveness using backward injection holes. In: Proc. ASME Turbo Expo 2015 Turbine Tech. Conf. Expo. GT2015 June 15 – 19, 2015, Montréal, Canada; 2015. p. 1–9.
- [25] Chen AF. Film Cooling with Forward and Backward Injection for Cylindrical and Fan-Shaped Holes using Psp Measurement Technique. Texas A&M University; 2013. <http://dx.doi.org/10.1115/GT2014-26232>.
- [26] Singh K, Premachandran B, Ravi MR. Experimental assessment of film cooling performance of short cylindrical holes on a flat surface. *Heat Mass Transf* 2016.
- [27] Kline SJ, McClintock FA. Describing uncertainties in single-sample experiments. *J Mech Eng* 1953;3–8.
- [28] Patankar SV. Numerical heat transfer and fluid flow. Washington DC: Hemisphere; 1990.
- [29] Sinha AK, Bogard DG, Crawford ME. Film-cooling effectiveness downstream of a single row of holes with variable density ratio. *J Turbomach* 1991;113:442. <http://dx.doi.org/10.1115/1.2927894>.
- [30] El-Gabry LA, Heidmann JD. Numerical study on the sensitivity of film cooling CFD results to experimental and numerical uncertainties. *Int J Comput Methods Eng Sci Mech* 2013;14:317–28. <http://dx.doi.org/10.1080/15502287.2012.756953>.
- [31] Singh K, Premachandran B, Ravi MR, Suresh B, Vasudev S. Prediction of film cooling effectiveness over a flat plate from film heating studies. *Numer Heat Transf Part A Appl* 2016;69:529–44. <http://dx.doi.org/10.1080/10407782.2015.1090232>.
- [32] Yao Y, Zhang J, Yang Y. Numerical study on film cooling mechanism and characteristics of cylindrical holes with branched jet injections. *Propuls Power Res* 2013;2:30–7. <http://dx.doi.org/10.1016/j.jppr.2012.12.001>.
- [33] Li G, Zhu H, Fan H. Discharge coefficient of 3-in-1 hole with various inclination angle and hole pitch. *Chin J Aeronaut* 2008;21:385–92. [http://dx.doi.org/10.1016/S1000-9361\(08\)60050-3](http://dx.doi.org/10.1016/S1000-9361(08)60050-3).
- [34] Li G, Wu C, Zhang W, Kou Z, Peng D. Effect of cross-flow direction of coolant on film cooling effectiveness with one inlet and double outlet hole injection. *Propuls Power Res* 2012;1:71–7. <http://dx.doi.org/10.1016/j.jppr.2012.10.006>.
- [35] Taslim M, Ugarte S. Discharge coefficient measurements for flow through compound-angle conical holes with cross-flow. *Int J Rotat. Mach* 2004;10: 145–53. <http://dx.doi.org/10.1080/10236210490277132>.